1975

I. Electronic crystal spectra for tetraammineplatinum (II) tetrachloroplatinate (II), potassium tetrachloropalladate (II), and potassium tetrabromopalladate (II); II. Crystal structure of potassium tetrabromoplatinate (II)

Rhonda Marie Rush
Iowa State University

INFORMATION TO USERS

This material was produced from a microfilm copy of the original document. While the most advanced technological means to photograph and reproduce this document have been used, the quality is heavily dependent upon the quality of the original submitted.

The following explanation of techniques is provided to help you understand markings or patterns which may appear on this reproduction.

1. The sign or "target" for pages apparently lacking from the document photographed is "Missing Page(s)". If it was possible to obtain the missing page(s) or section, they are spliced into the film along with adjacent pages. This may have necessitated cutting thru an image and duplicating adjacent pages to insure you complete continuity.

2. When an image on the film is obliterated with a large round black mark, it is an indication that the photographer suspected that the copy may have moved during exposure and thus cause a blurred image. You will find a good image of the page in the adjacent frame.

3. When a map, drawing or chart, etc., was part of the material being photographed the photographer followed a definite method in "sectioning" the material. It is customary to begin photoing at the upper left hand corner of a large sheet and to continue photoing from left to right in equal sections with a small overlap. If necessary, sectioning is continued again — beginning below the first row and continuing on until complete.

4. The majority of users indicate that the textual content is of greatest value, however, a somewhat higher quality reproduction could be made from "photographs" if essential to the understanding of the dissertation. Silver prints of "photographs" may be ordered at additional charge by writing the Order Department, giving the catalog number, title, author and specific pages you wish reproduced.

5. PLEASE NOTE: Some pages may have indistinct print. Filmed as received.

Xerox University Microfilms
300 North Zeeb Road
Ann Arbor, Michigan 48106

I. Electronic crystal spectra for tetraammineplatinum(II) tetrachloroplatinate(II), potassium tetrachloropalladate(II), and potassium tetrabromopalladate(II).

II. Crystal structure of potassium tetrabromoplatinate(II).

by

Rhonda Marie Rush

A Dissertation Submitted to the
Graduate Faculty in Partial Fulfillment of
The Requirements for the Degree of
DOCTOR OF PHILOSOPHY

Department: Chemistry
Major: Inorganic Chemistry

Approved:

Signature was redacted for privacy.

In Charge of Major Work

Signature was redacted for privacy.

For the Major Department

Signature was redacted for privacy.

For the Graduate College

Iowa State University
Ames, Iowa

1975

TABLE OF CONTENTS

PREFACE

This thesis is divided into two areas of research - spectroscopy and crystallography. The crystal structure determination has been presented in part IV. The spectral studies comprise a greater part of this thesis. The Introduction and Experimental sections are devoted to spectroscopy. In part III, the results of each compound are presented and are discussed with respect to the current literature. In the discussion of a transition, the peak location determined in this study may be slightly different than that reported by another author. The literature values have not been changed to correspond to wave numbers obtained in this study.

I. INTRODUCTION

The purpose of this research was to obtain and interpret the polarized crystal spectra for tetraammineplatinum(II) tetrachloroplatinate(II), commonly called Magnus' green salt, potassium tetrachloropalladate(II), and potassium tetrabromopalladate(II). These coordination complexes of platinum(II) and palladium(II) have a square-planar geometry and are diamagnetic having a $5d^8$ or $4d^8$ electronic configuration, respectively. In the solid state these square-planar ions are aligned directly over one another in columnar arrays. Since in crystals the complexes have a known orientation, absorption spectra with plane polarized light can provide some definitive assignments for transitions in these d^8 systems. The electronic absorption spectra provides information about the crystal interactions and possible solid state effects. For crystals with large metal-metal separations as in K_2PdCl_4 and K_2PdBr_4, the spectra correlate closely with the solution spectra. For Magnus' green salt (MGS), the spectral assignments are consistent with large energy shifts of the transitions due to crystal effects. The data and assignments presented in this thesis complement a series of studies made on square-planar platinum(II) complexes (1,2).

In particular, the spectral studies presented parallel the work reported for K_2PtCl_4 and K_2PtBr_4. Studies of these platinum(II) complexes have provided a great deal of

information about molecular energy levels. The K_2PtCl_4 structure possessed by both these salts is optimal for polarized crystal spectra and is shown in Figure 1. The anion sits in a site of full D_{4h} symmetry (3,4).

Because of the high symmetry of $PtCl_4^{2-}$, extensive theoretical studies have been possible. There has not been an unanimity of opinion on the transition assignments or on the ordering of the molecular orbitals. However, Chatt, Gamlen and Orgel (5) first assigned a number of transitions for $PtCl_4^{2-}$ as excitations of d electrons. From the aqueous solution spectra, they proposed a metal d-orbital ordering scheme which qualitatively ordered the platinum orbital energies as $d_{z^2}<d_{xz}=d_{yz}<d_{xy}<d_{x^2-y^2}$. This ordering is representative of an axis system where the x and y axes lie along the Pt-Cl bonds, the z axis is perpendicular to the planar ion. Fenske, Martin and Ruedenberg (6) attempted to determine the d-orbital ordering using an effective point dipole model for ligand field interactions. This method calculated quantitative values for the electron repulsion interactions in terms of Slater-Condon F parameters. The ordering proposed by Fenske et al. was $d_{xz}=d_{yz}<d_{z^2}<d_{xy}<d_{x^2-y^2}$.

Gray and Ballhausen (7) used linear combinations of atomic orbitals in their self-consistent charge and configuration molecular orbital approach to assign the

Figure 1. A unit cell for the tetragonal K_2PtCl_4 structure. K ions are at z = 1/2, others are at z = 0.

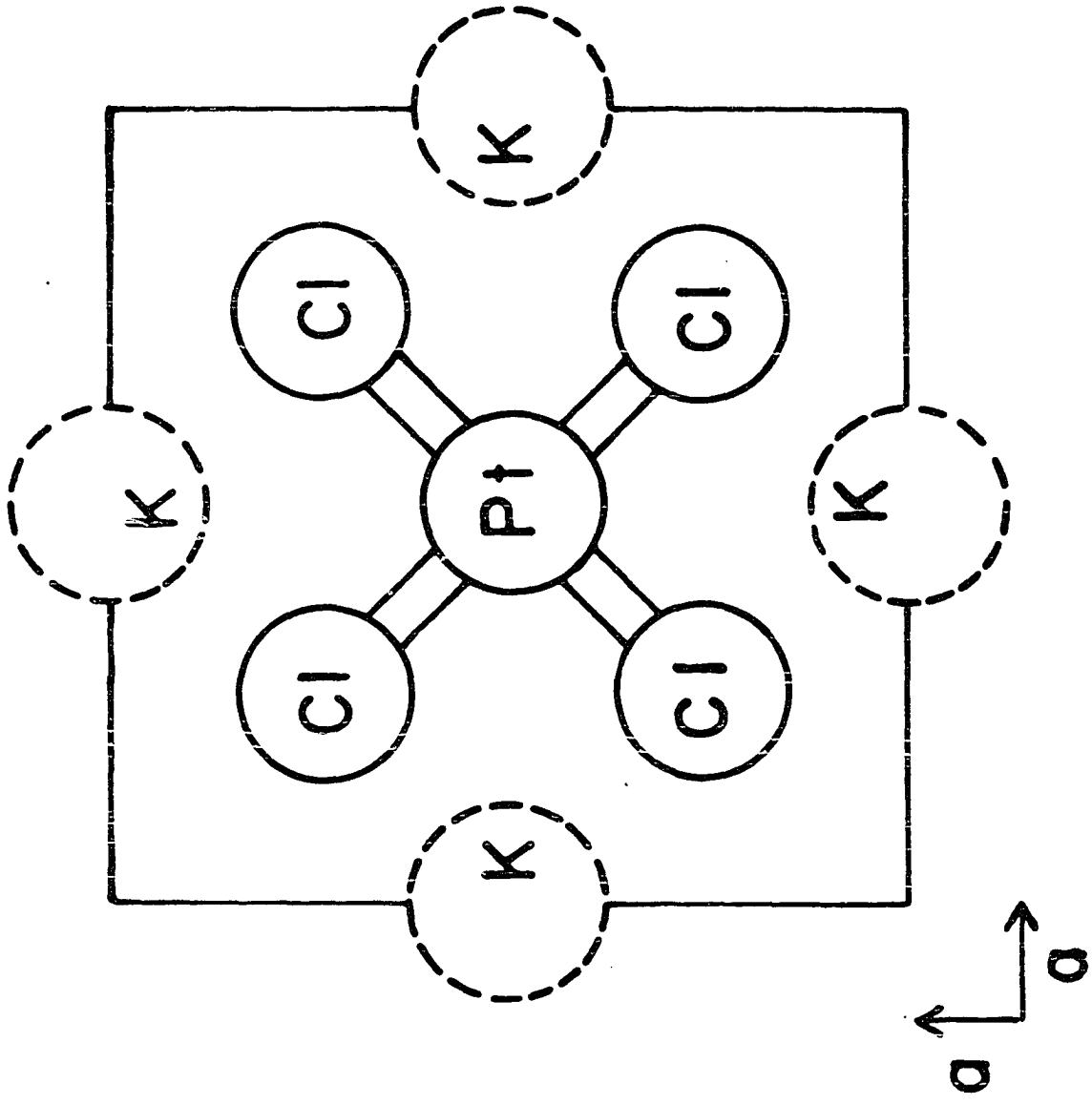
K
Cl
Cl
K
Pt
K
Cl
Cl
K
a
a

transitions of $PtCl_4^{-2}$. In their method the overlap integrals were evaluated and the d-orbital ordering was the same as that proposed by Fenske et al. (6). Semi-empirical molecular orbital treatments were also reported by Basch and Gray (8) and by Cotton and Harris (9). Cotton and Harris also used nodeless Slater-type orbitals. Parameters were fitted to give the best value of the overlap integral. In the final calculation for orbital energies, Cotton and Harris (9) made use of an extended Hückel-type calculation. Their results were in agreement with the d-orbital ordering proposed by Chatt et al. (5).

Despite the insights gained by such calculations, spectroscopic assignments could not be made from theory alone with impunity. Obviously, there were conflicts in the proposed ordering which could not be settled by using the solution spectra alone.

Many spectral studies of tetrachloroplatinate(II) have been reported which included a variety of transition assignments (10-15). The first definitive work was reported in 1966 when Martin, Foss, McCarville, Tucker and Kassman (16) reported the magnetic circular dichroism (MCD) spectrum of K_2PtCl_4 solution. Martin, Tucker and Kassman (17) reported polarized single crystal spectra at 15°K and proposed transition assignments supporting the d-orbital ordering in Figure 2. These studies by Martin and coworkers (14,16,17)

were later complemented by the MCD solution studies of McCaffery, Schatz and Stephens (18). These definitive studies supported the original d-orbital ordering proposed by Chatt, Gamlen and Orgel (5).

From experimental and theoretical studies on $PtCl_4^{2-}$, a molecular orbital (MO) diagram for the spectroscopically relevant orbitals is shown in Figure 2. The connecting lines in the diagram identify the principal component of each MO. The lowest unfilled orbital is the antibonding orbital b_{1g}-σ^*, based on the $d_{x^2-y^2}$ metal orbital. The highest filled orbital is the b_{2g}, based on the d_{xy} and is considered to be π antibonding in character. The e_g-$d_{xz,yz}$ is π antibonding in character; the a_{1g}-d_{z^2} orbital has the capability for sigma bonding. It should be recognized that orbitals of the same symmetry mix somewhat. The p-orbitals of the ligands have been proposed for bonding. There are twelve symmetry adapted linear combinations of which only the ungerade combinations have been included in Figure 2.

An absorption transition for these diamagnetic complexes can be viewed as one electron being transferred from a doubly occupied orbital to an empty orbital. The optical absorption transition can be characterized by a transition dipole moment given as

$$r = \int \psi^*_{Gr} \hat{R} \psi_{Ex} \, d\tau \qquad (1)$$

Figure 2. The molecular orbital scheme for a platinum(II) complex under D_{4h} symmetry as in $PtCl_4^{2-}$ or $PtBr_4^{2-}$. Only the p orbitals of the halides have been included and gerade orbitals arising from ligand π and σ orbitals have been omitted. On the right are the excited symmetry states arising from d←d transitions from the $^1A_{1g}$ ground state. Both singlet and triplet states will occur for each of the indicated symmetry states.

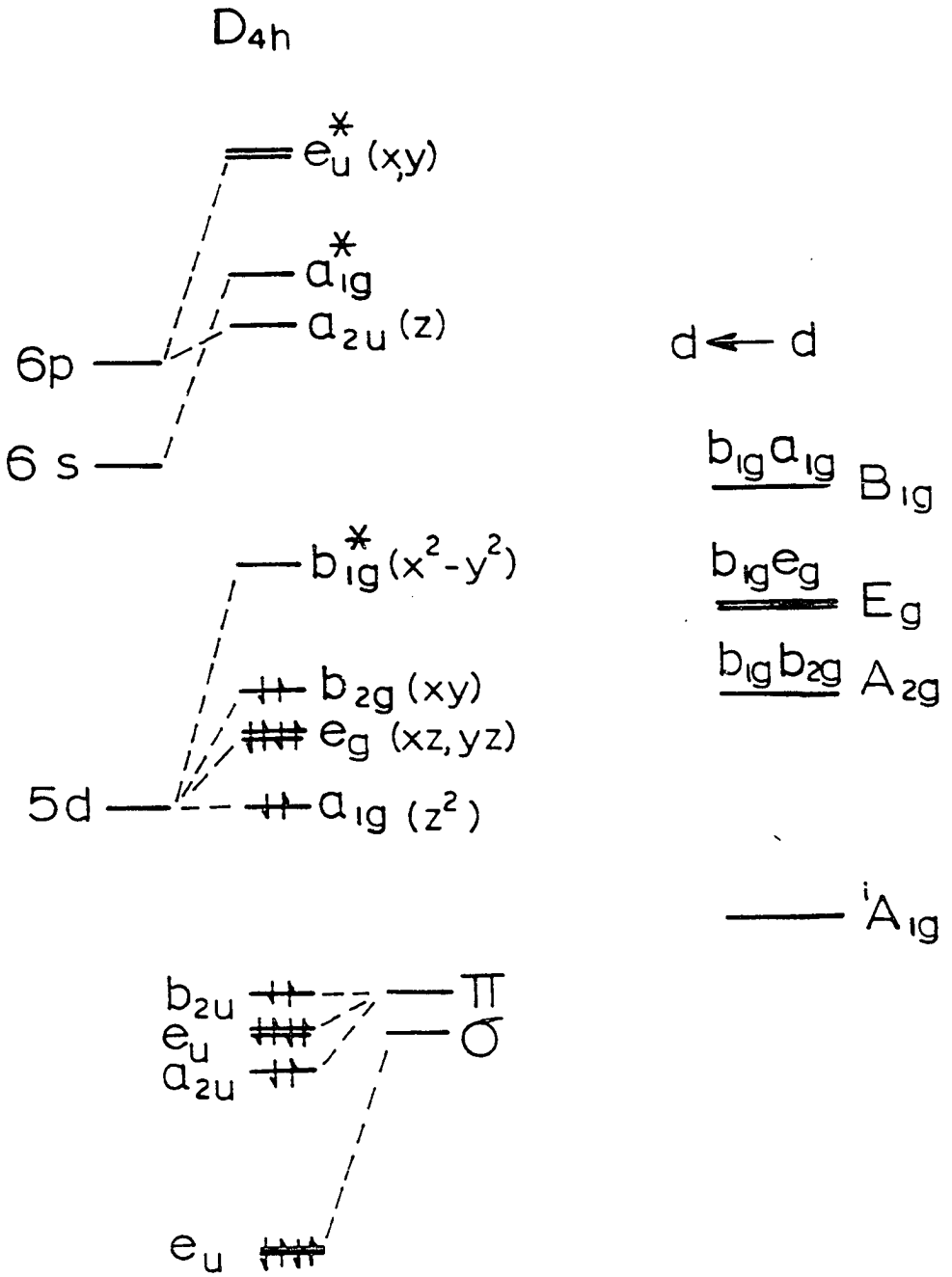
D4h
e*u (x,y)
a*1g
a2u (z)
6p
6 s
b*1g (x²-y²)
b2g (xy)
eg (xz, yz)
5d
a1g (z²)
b2u
eu
a2u
π
σ
eu
d ← d
b1g a1g B1g
b1g eg Eg
b1g b2g A2g
¹A1g

where ψ_{Gr} and ψ_{Ex} are the ground and excited state wave functions and $\hat{R}$ is the one electron dipole operator. Selection rules are derived from the symmetries of the terms in equation 1. The ground state wave function has $^1A_{1g}$ symmetry since all electrons are paired. The dipole operator has three components $\hat{R}_x$ and $\hat{R}_y$, which in D_{4h} form a basis function for E_u, and $\hat{R}_z$, which forms a basis for A_{2u}. The excited state symmetry is the product of the symmetries of the initial and final orbitals, u_i and u_f.

For an allowed transition that has a non-zero dipole moment integral, the products of the terms in equation 1 must contain a basis for the totally symmetric irreducible representation, A_{1g}. Hence the $^1A_{2u} \leftarrow {}^1A_{1g}(b_{1g}-\sigma^* \leftarrow b_{2u}-L\pi)$ transition will be dipole allowed in the z-polarization. Likewise, the $^1E_u \leftarrow {}^1A_{1g}(b_{1g}-\sigma^* \leftarrow e_u-L\pi)$ and the $^1E_u \leftarrow {}^1A_{1g}(b_{1g}-\sigma^* \leftarrow e_u-L\sigma)$ transitions will be dipole allowed in the x,y-polarization. Other transitions will be forbidden. An estimate of the transition dipole moment can be obtained from intensities which are usually expressed as oscillator strengths (19).

In Figure 2 the possible d←d transitions are listed. These transitions are Laporte forbidden, and have smaller oscillator strengths than the dipole allowed transitions. The allowedness of the d←d transitions is generally attributed to the removal of the exact inversion center in the square-planar ion. The removal of the inversion center may result

from local asymmetries arising from crystal fields due to neighboring ions or molecules. This is not applicable for the case of K_2PtCl_4 or K_2PtBr_4. Asymmetric molecular vibrations may serve as perturbations to remove the inversion center and reduce the symmetry. The momentary symmetry reduction permits otherwise forbidden transitions to be "partially" allowed. The vibronic model has been applied by Martin and coworkers (1,14,17) to specify the non-zero transition moment integrals which result from the asymmetric vibrations, and thus to develop selection rules for K_2PtCl_4 and K_2PtBr_4.

In Figure 3 the excited states for both salts are compared. Below 30,000 cm^{-1} the d←d transitions in K_2PtBr_4 fell 1,500 to 2,200 cm^{-1} below the corresponding bands of K_2PtCl_4. The character of the bands was similar in that the same transitions had exhibited the vibrational structure (20). For both salts the d←d transitions below 30,000 cm^{-1} had lower peak heights and were narrower at lower temperatures. These features were consistent with their excitation by the vibronic mechanism since the average vibrational amplitude and hence the magnitude of the asymmetric perturbation are reduced at lower temperature. One difference between the two salts was the relative intensities for alternate polarizations (20). For K_2PtBr_4 the bands in x,y-polarization were generally more intense

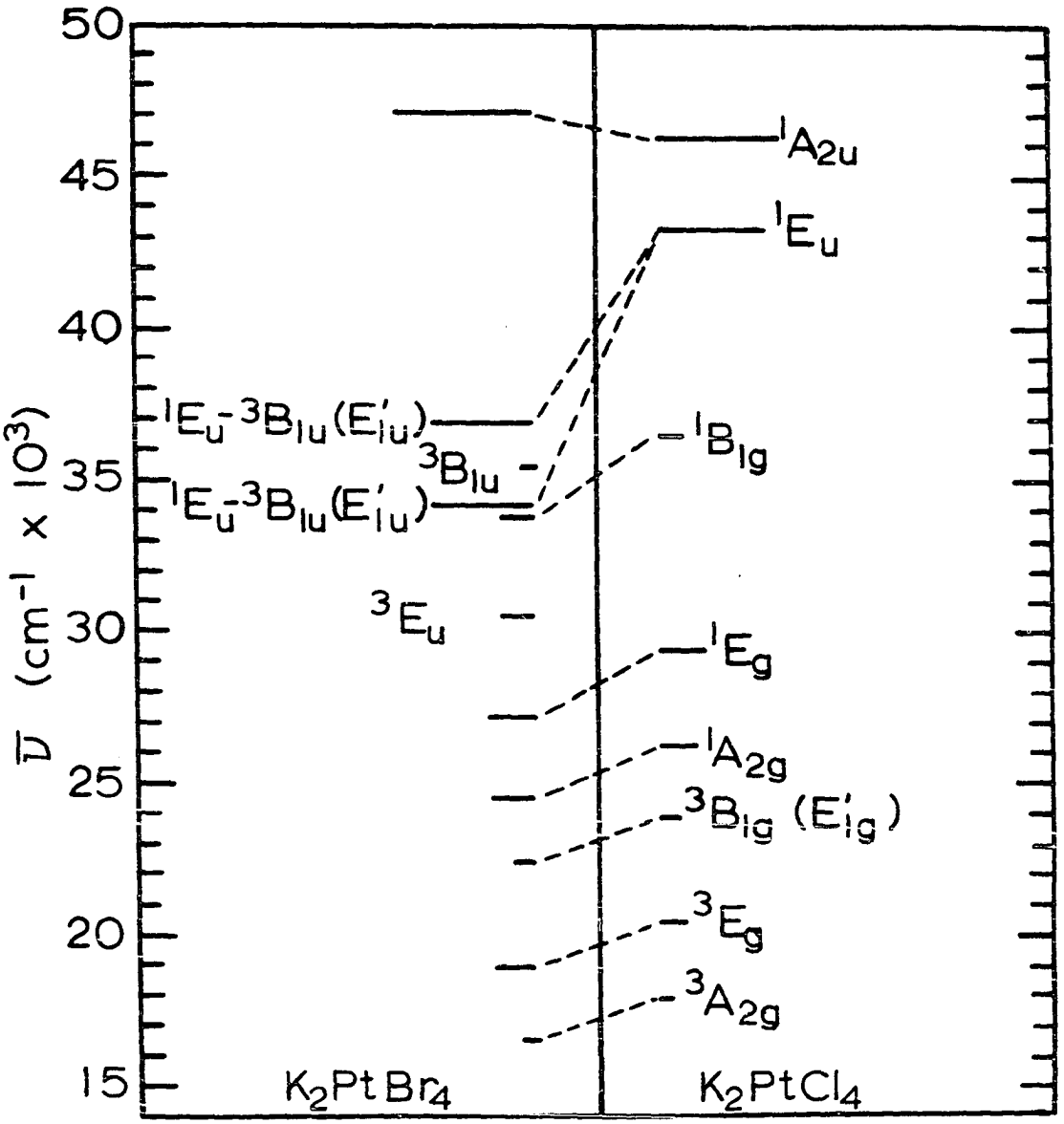

Figure 3. Comparison for excited states of K_2PtBr_4 and K_2PtCl_4. The length of line for each state is proportional to log ϵ_{max} (15°) for the crystal transitions and log ϵ_{max} (soln) for the intense transitions.

than those in z-polarization; the opposite was true for K_2PtCl_4. This implied that the $^1E_u \leftarrow {}^1A_{1g}$ transitions from which the forbidden d←d transitions borrow intensity in x,y-polarization had moved to lower energies in K_2PtBr_4 (20).

The lowest energy spin-allowed transition was the $^1A_{2g} \leftarrow {}^1A_{1g}(b_{1g}-\sigma^* \leftarrow b_{2g}-d_{xy})$, which was absent in the z-polarization; and vibrational structure was resolved on the band at 15°K (17,21). Identification of the $^1A_{2g} \leftarrow {}^1A_{1g}$ transition was based on the selection rules (1) which require this transition to occur only in x,y-polarization. The $^1E_g \leftarrow {}^1A_{1g}(b_{1g}-\sigma^* \leftarrow e_g-d_{xz,yz})$ transition was at 29,400 cm^{-1} for K_2PtCl_4; this assignment was confirmed by the MCD solution spectrum (18). For K_2PtBr_4 the $^1E_g \leftarrow {}^1A_{1g}$ transition was assigned by analogy with K_2PtCl_4. Accordingly, the $^3A_{1g}$ and ^3E_g states were assigned some 8000 cm^{-1} lower in energy. The large spin-orbit coupling of the platinum accounts for the high intensities of these spin-forbidden transitions (20). For K_2PtBr_4 at 15°K a shoulder was resolved at ca. 22,700 cm^{-1} which exhibited vibrational structure in both polarizations, as shown in Figure 4. The assignment to the $^3B_{1g} \leftarrow {}^1A_{1g}$ transition seemed logical and consistent with the luminescence spectrum of Cs_2PtCl_4 in Cs_2ZrCl_6 (21) and the polarized spectra of K_2PtCl_4 (17).

The $^1B_{1g} \leftarrow {}^1A_{1g}(b_{1g}-\sigma^* \leftarrow a_{1g}-d_{z^2})$ transition was possibly observed for K_2PtCl_4 as a shoulder on a rapidly rising

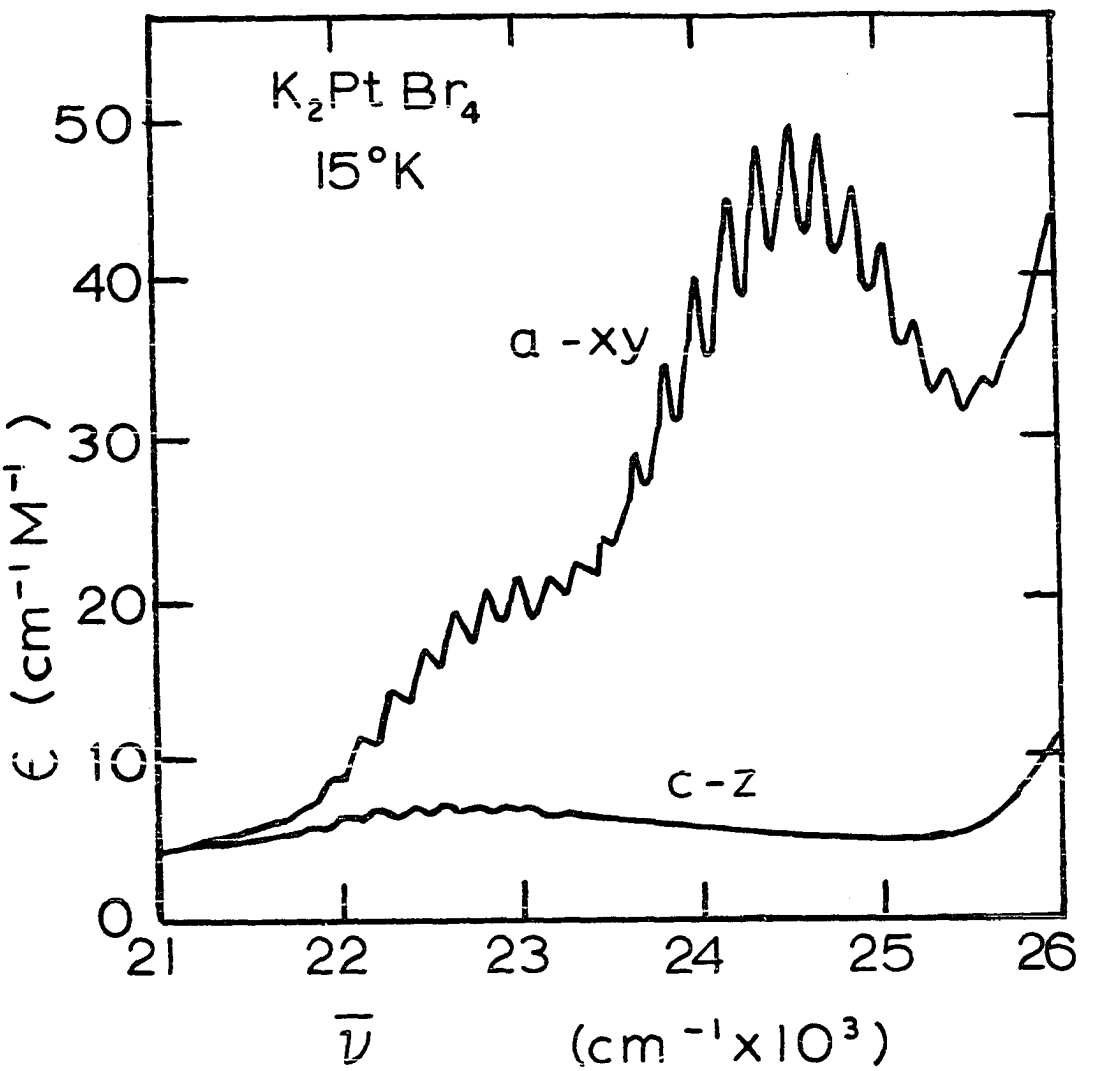

Figure 4. Section of the 15°K spectrum for K_2PtBr_4 which exhibits vibrational structure. The crystal was 26 μ thick.

absorption at ca. 36,500 cm^{-1} (20). In Figure 5 this component appeared in both polarizations at 15°K. The band occurs on steeply rising absorption regions so its temperature dependence cannot be established. This state is ca. 12,500 cm^{-1} higher in energy than the state assigned as $^3B_{1g}$. Likewise, a possible $^1B_{1g} \leftarrow {}^1A_{1g}$ transition was observed in thin crystals of K_2PtBr_4. The band appeared as a shoulder in z-polarization at ca. 33,800 cm^{-1} as shown in Figure 6. The assignment seemed reasonable since again a transition which can be assigned as the $^3B_{1g} \leftarrow {}^1A_{1g}$ was observed at ca. 22,700 cm^{-1}; the singlet-triplet state separations were 11,100 cm^{-1} for K_2PtBr_4 (20).

The high energy transitions for K_2PtCl_4 and K_2PtBr_4 are considerably different. McCaffery et al. (18) showed that there was an MCD-A term associated with the shoulder at 43,400 cm^{-1} for $PtCl_4^{2-}$. No A term was evident for the peak at 46,400 cm^{-1}. Anex and Takeudhi (22) reported that the 46,000 cm^{-1} band was out-of-plane or z-polarized. The band at 43,400 can be assigned to the $^1E_u \leftarrow {}^1A_{1g}(a_{2u}\text{-}p_z \leftarrow e_g\text{-}d_{xz,yz})$ transition and the band at 46,400 cm^{-1} can be assigned to the $^1A_{2u} \leftarrow {}^1A_{1g}(a_{2u}\text{-}p_z \leftarrow a_{1g}\text{-}d_{z^2})$ transition. For $PtBr_4^{2-}$ the $p_z \leftarrow d$ state energies have moved higher, whereas the $\sigma^* \leftarrow L$ energies have moved lower. An intense $^1A_{2u} \leftarrow {}^1A_{1g}$ transition cannot occur below 48,100 cm^{-1} (20). For $PtBr_4^{2-}$ there are two intense bands at 34,200 and 37,000 cm^{-1} in x,y-polarization.

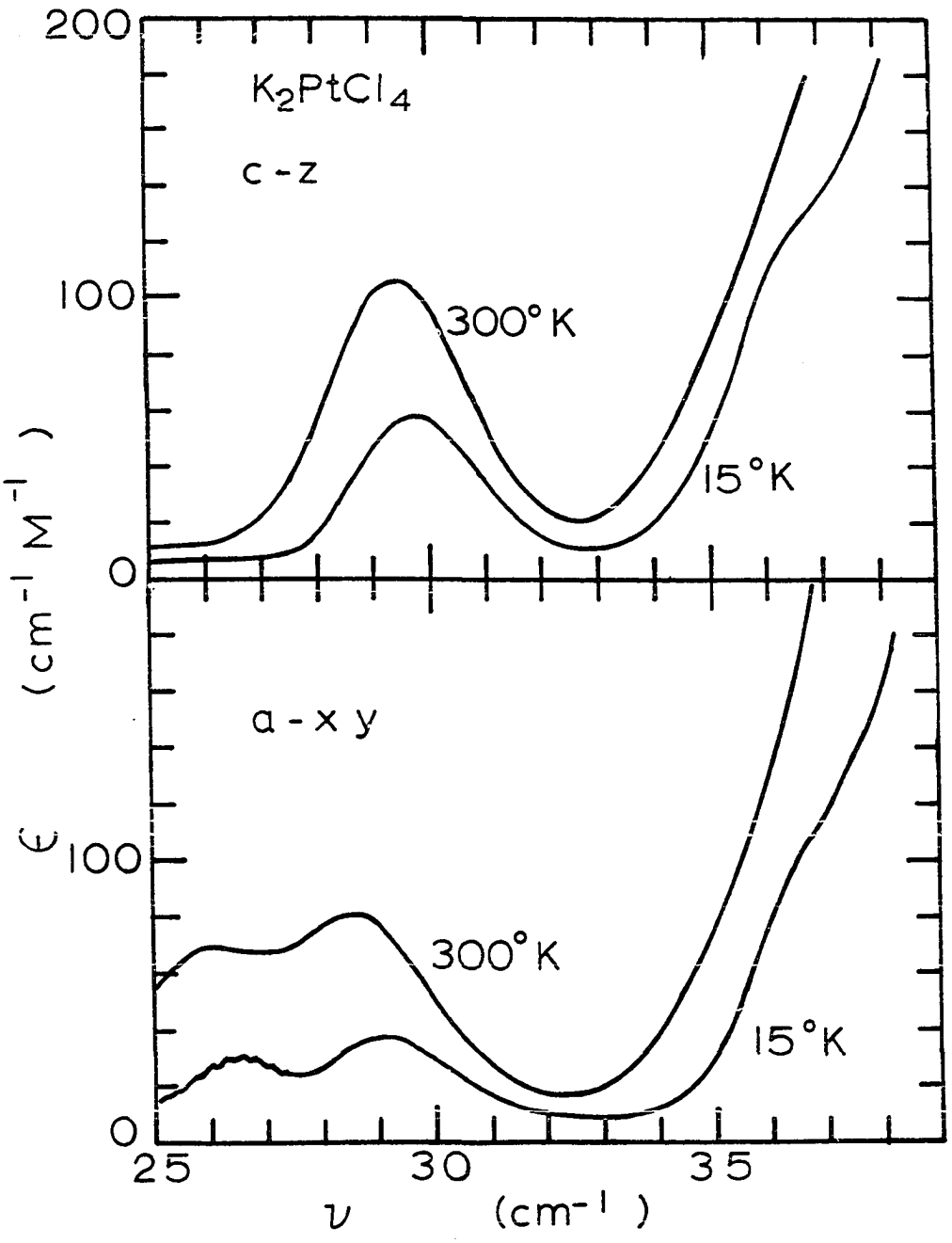

Figure 5. Portions of the polarized crystal spectra at 300° and 15°K for a crystal of K_2PtCl_4, 15 μ thick.

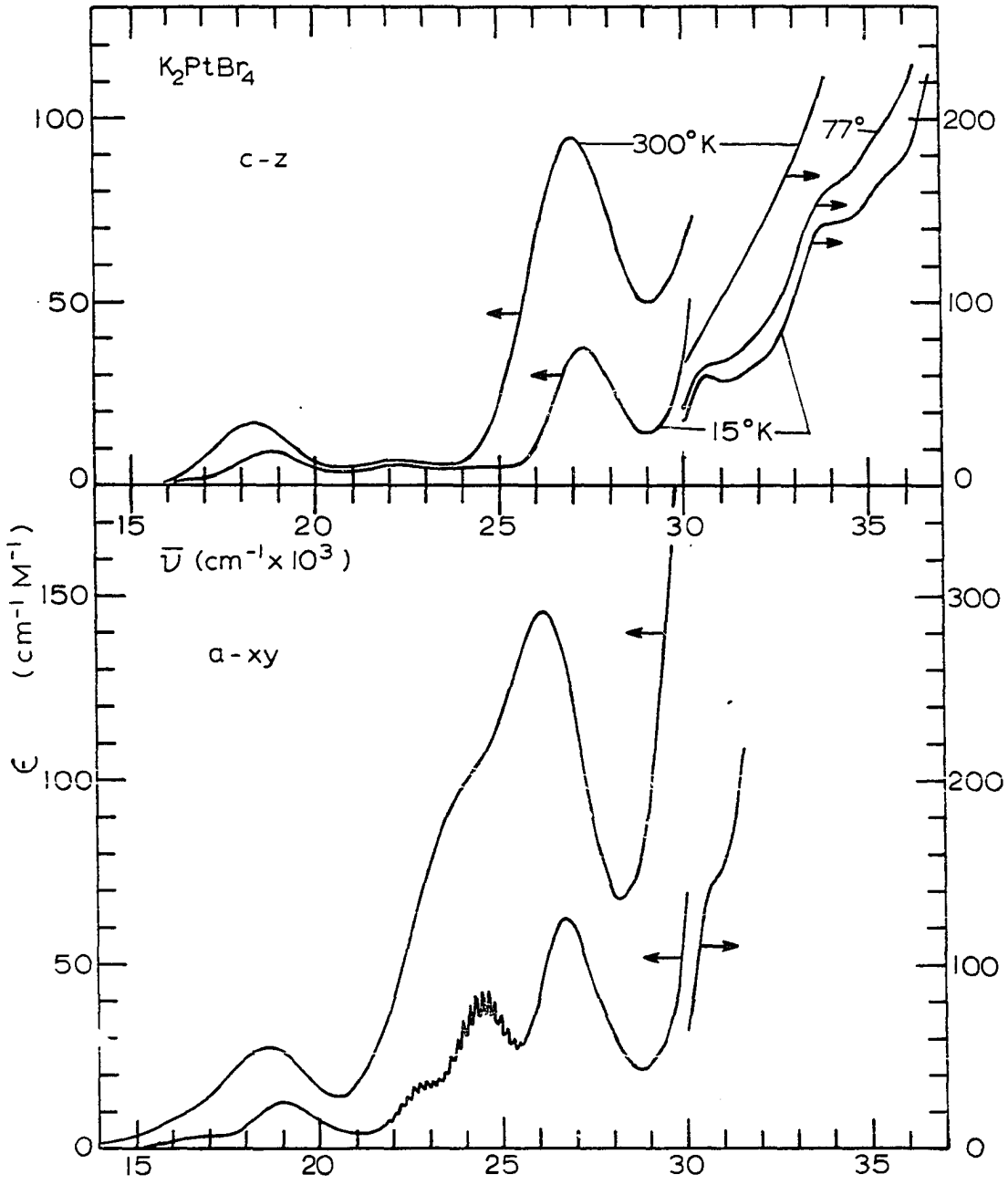

Figure 6. Polarized crystal spectra for K_2PtBr_4. From 14,000 to 30,000 cm^{-1} the crystal was 26 μ thick. Above 30,000 cm^{-1} the spectrum is for a crystal which was 11.5 μ thick.

The presence of these two bands was explained by the near coincidence of a triplet and ^1E_u state which were mixed by spin-orbit coupling of the platinum and bromine atoms. The splitting of 3,000 cm^{-1} between the bands at 34,200 and 37,200 cm^{-1} appears reasonable for spin-orbit interactions (20). For K_2PtBr_4 and K_2PtCl_4, the differences in the intense transitions were striking. For $PtCl_4^{2-}$ the strong $^1A_{2u} \leftarrow {}^1A_{1g}$ transition lies close in energy to the lowest $^1E_u \leftarrow {}^1A_{1g}$; however, for $PtBr_4^{2-}$ these states were separated some 11,000 cm^{-1}. It seemed that the intense transitions probably cannot be described as pure $\sigma^* \leftarrow L$ or $p \leftarrow d$ transitions but rather with some mixture of both.

Patterson, Godfrey and Khan (21) reported the sharp-line luminescence and absorption spectra for Cs_2PtCl_4 doped in single crystals of Cs_2ZrCl_6. The mole percent of platinum complex was 0.1-1%. The absorption spectra for K_2PtCl_4 and Cs_2PtCl_4-Cs_2ZrCl_6 was recorded from 16,500 to 27,000 cm^{-1} at 4°K. The vibrational fine structure for K_2PtCl_4 appeared broad while that for the guest $PtCl_4^{2-}$ in the Cs_2ZrCl_6 host was sharp and structured. The observed structure consisted of progressions in which the symmetric stretching mode was coupled to odd modes of the $PtCl_4^{-2}$ anion in its ground electronic state. There was a shift of 50 cm^{-1} for the $^1A_{2g} \leftarrow {}^1A_{1g}$ band origin in the cesium salt compared to this origin in K_2PtCl_4.

The spectrum for Cs_2PtCl_4-Cs_2ZrCl_6 was analyzed in terms of the $PtCl_4^{-2}$ ion. Likewise, the spectrum for $[Pt(NH_3)_4][PtCl_4]$, (MGS) has been analyzed in terms of the $PtCl_4^{-2}$ ion by Day et al. (15). Because of the strong dichroism and deep green color of MGS, the present study was undertaken. In MGS there was a possibility of interionic electron-transfer transitions which may have had non-zero transition dipole moments (1). This type of transition would have a very different temperature dependence from transitions excited exclusively by a vibronic mechanism (23,24). To determine the nature of the absorption, polarized spectra were obtained at 15°K.

For K_2PdCl_4 and K_2PdBr_4 the dichroism was not as strong as in MGS. In these salts the anions were separated by more than 4.0Å (25,26). The spectra were obtained and interpreted in light of recent calculations by Katô (27) and Messmer, Interrante and Johnson (28). Katô reported MO calculations for $PtCl_4^{2-}$ and $PdCl_4^{2-}$; his orbital energy results were similar to those reported by Cotton and Harris (9), and Basch and Gray (8). However, Katô extended the calculations to include the analysis of band shape and signs for the MCD spectra (18), which he used in assigning the high energy transitions of $PtCl_4^{2-}$, $PdCl_4^{2-}$ and $PdBr_4^{2-}$ (27). In 1974 Messmer et al. (28) reported SCF-Xα-SW calculations for K_2PtCl_4 and K_2PdCl_4. Further details of these calculations

will be discussed as they apply to the palladium(II) compounds in this thesis.

II. EXPERIMENTAL

The palladium salts were prepared by modifying the procedures for the analogous platinum salts (29,30). The K_2PdCl_4 was prepared by oxidation of palladium black with aqua regia to form H_2PdCl_4. Careful addition of KOH until a pH of 2 was reached permitted the K_2PdCl_4 to crystallize from solution. The crystals were recrystallized from cold water and ethanol. Thermogravimetric analysis showed a weight loss to 580°C as Cl_2 of 21.9%, a loss to 800°C as KCl of 44.4% and a Pd residue of 33.7%. The calculated values were: Cl_2, 21.7%; KCl, 45.7%; Pd, 32.6%.

The K_2PdBr_4 was prepared by the addition of concentrated HBr to hot solutions of tetrachloropalladic(II) acid. This mixture was evaporated to dryness and the procedure was repeated. The volume of H_2PdBr_4 solution was reduced by evaporation before aqueous KOH was added to bring the pH to 2. Red crystallites of K_2PdBr_4 precipitated out of the solution. The mixture was filtered and the crystals were washed with cold absolute alcohol. Thermal gravimetric analysis showed a weight loss to 525°C as Br_2 of 31.9%, a weight loss to 745°C as KBr of 47.2%, and a Pd residue of 20.9% after 800°C. The calculated values were: Br_2, 31.7%; KBr, 47.2%; Pd, 21.1%.

The crystals of Magnus' green salt were grown by a diffusion-controlled precipitation from solutions of K_2PtCl_4 and $Pt(NH_3)_4Cl_2 \cdot H_2O$. The K_2PtCl_4 was prepared by the method

of Grantham et al. (31). The $Pt(NH_3)_4Cl_2 \cdot H_2O$ was prepared from K_2PtCl_4 by the addition of an excess of NH_3 and boiling until all of the initially formed Magnus' green salt had dissolved. After the excess ammonia had been boiled off, the volume was reduced and the salt was precipitated with the addition of an acetone-alcohol-ether mixture. The $Pt(NH_3)_4Cl_2 \cdot H_2O$ was stored in the dark after it was recrystallized.

Milligram quantities of K_2PtCl_4 and $Pt(NH_3)_4Cl_2 \cdot H_2O$ were placed on opposite corners of one 5-cm silica plate. A drop of water was placed in the center of the plate and a second plate was pressed down on the first until the salts had dissolved. The plates were stored and crystals of MGS normally formed in about three days. Although many tiny crystals formed, a few were large enough for spectral studies.

Thin crystals of K_2PdCl_4 and K_2PdBr_4 used for spectral studies were grown by evaporation of a film of solution between polished silica plates. After the crystals formed, the plates were exposed to room air so that excess water evaporated to permit easy separation of the plates. The crystals were routinely less than 25 microns thick, and some were large enough to cover pinholes which were 75-150 microns in diameter.

A single crystal was loosened from the plate using absolute or 95% ethanol and then it was transferred on a needle to a platinum metal pinhole plate. A small amount of

silicone vacuum grease was spread near one segment of the pinhole and the crystal was pushed until one edge contacted the grease. The grease successfully held light crystals over the pinhole. The crystal on the pinhole was re-examined to make sure it covered the hole and that no grease had seeped into the hole. Thicker crystals were picked out of evaporating dishes. When found to be single and large enough to cover pinholes, they were mounted and a varnish was used in place of grease.

For spectrophotometric measurements the platinum pinhole plate was mounted in either a cryostat or on a holder which was placed in beneath a rotating microscope stage on the rotation axis of the stage. The polarized spectra were recorded by a Cary 14 spectrophotometer with Glan calcite polarizers in both the reference and sample beams. This balanced out any polarizer effects caused by either calcite absorption bands or systematic polarization within the instrument. A high intensity light source, Model 1471200, was used from 650 nm to about 280 nm. The hydrogen arc was used in the ultraviolet spectrum from 280 to 190 nm. In the cryostat it was possible to mount the pinhole plate directly against the copper block which formed the bottom of the vacuum-insulated can. The cryogenic spectra were obtained by adding liquid nitrogen, 77°K, and then replacing it with liquid helium to provide a nominal temperature of 15°K.

For each spectrum a reference line was scanned with a comparable pinhole in the sample compartment. Occasionally, individual reference traces were somewhat variable. This feature introduced some uncertainty into individual measurements, especially in regions of low absorbance. For these complexes the major spectral features were duplicated several times in scans of more than 15 different crystals for MGS, 31 for K_2PdCl_4, and 26 for K_2PdBr_4. The spectral and baseline data were automatically punched on computer cards by a Cary-Datex digitalization system. The spectra were plotted using IPLOT (32).

Molar absorptivities were determined from the absorbance divided by the concentration and crystal thickness. Molar concentrations were calculated from the crystal density and unit cell volume as: MGS, 6.28 M; K_2PdCl_4, 8.07 M; K_2PdBr_4, 7.51 M. The crystal absorbance was obtained by subtracting the reference absorbance from the sample absorbance at a particular wave length. To fix the absorbance scale, it was necessary to scan into a region of negligible absorption. If the crystal was large and weighed over 150 mg, a weight and area determination was used to determine the thickness (33). Another method required the use of a Bausch and Lomb traveling microscope to measure the crystal thickness directly. The thicknesses obtained by these two methods had an uncertainty of as much as 10 to 20%. Since most of the

crystals were tiny, an interference method based on multiple internal reflection was developed to establish the thickness for standard crystals. However, this method requires indices of refraction for the crystals.

Tetragonal crystals such as K_2PdCl_4, K_2PdBr_4 and MGS are uniaxial. A light ray entering a crystal breaks into two rays which have different refractive indices. There is a refractive index for light polarized along the crystallographic c-axis, n_c or n_E. Likewise, the refractive index is n_a or n_O for light polarized in the a-direction. The refractive indices of crystals may be determined by the Becke line method which utilizes a polarizing microscope. When a crystal is immersed in a liquid, it is possible to tell quite precisely whether the crystal index or the liquid index is larger by the motion of the Becke line upon focusing the microscope (34). The index for the liquid can be changed by mixing two liquids whose indices bracket the crystal index until a matching is obtained. Care must be taken to control the temperature of the immersion liquid and to use a constant, monochromatic light source. The Becke line method is more sensitive if the observations are made using a high quality polarizing microscope with a low aperture.

Direct measurement of the refractive indices for MGS and of n_a for K_2PdBr_4 was not feasible since these indices were greater than the index of methylene iodide, 1.74, which was the highest index of a conveniently available and suitable liquid.

Both indices of K_2PdCl_4 and n_c in K_2PdBr_4 were below 1.74. A standard procedure (34) was used to measure liquid indices using a Bausch and Lomb Precision Refractometer equipped with a sodium lamp and thermostated at 25°C. The Becke line method indicated that n_a for K_2PdCl_4 was greater than 1.658 by immersion in α-bromonaphthalene, but n_c was less than 1.658. A match for n_c was found for a liquid with a refractive index of 1.5389 at 25°C at 5893Å. Although a match for n_a was found, the liquid was too high for the scale on the refractometer. For K_2PdBr_4, n_c was determined as 1.5808. The interference method was developed to determine the higher refractive indices.

The interference method for determining crystal thickness was developed because sometimes during the recording of a spectrum, periodic fluctuations or waves were observed in the regions of low absorbance. These absorbance waves were observed in spectra for crystals which had well-developed hk0 faces of high optical quality. Figure 7 indicated a path or a light ray in a crystal. A light wave, entering an incident face, was partially reflected and refracted at each crystal face. The phenomenon was explained by following the path or a light ray through a crystal to the emergent face. There the wave was partially reflected and returned to the incident face where again it was partially reflected. A doubly reflected light wave interfered with subsequent entering

light waves traversing the crystal. Multiple reflections occurring within a crystal therefore gave rise to the observed phenomena. A limited recording of absorbance versus wave length for the a-polarization of MGS was reproduced in Figure 8.

A minimum in the absorbance waves represented constructive interference for the transmitted and internally reflected light rays (35). At the minima the thickness of a crystal was

$$L = N/(2\bar{\nu}_N n_N) \tag{2}$$

where N was the integral number of wave lengths needed to traverse two crystal thicknesses and n_N was the refractive index for that crystal at $\bar{\nu}_N$ in that polarization. The wave lengths were determined to within about ± 1-2 Å from slow spectral scans. The wave numbers for the observed minima or maxima were determined and designated as $\bar{\nu}_M$ where M was N+m. So, m had integral values for minima and half integral values for maxima.

The variable $\bar{\nu}_M$ was fitted to M by a quadratic least-squares. From equation 2, it followed that

$$(N+m)/N = 1+m/N = n_M\bar{\nu}_M/n_N\bar{\nu}_N = [1+(\bar{\nu}_M-\bar{\nu}_N)/\bar{\nu}_N][1+(n_M-n_N)/n_N]. \tag{3}$$

Rearrangement of equation 3 gave

$$m\bar{\nu}_N/(\bar{\nu}_M-\bar{\nu}_N) = N+N[(n_M-n_N)/(\bar{\nu}_M-\bar{\nu}_N)]\bar{\nu}_M/n_N \tag{4}$$

and

$$\lim_{m\to 0} m\bar{\nu}_N/(\bar{\nu}_M-\bar{\nu}_N) = N+N(dn/d\bar{\nu})_N\bar{\nu}_M/n_N. \tag{5}$$

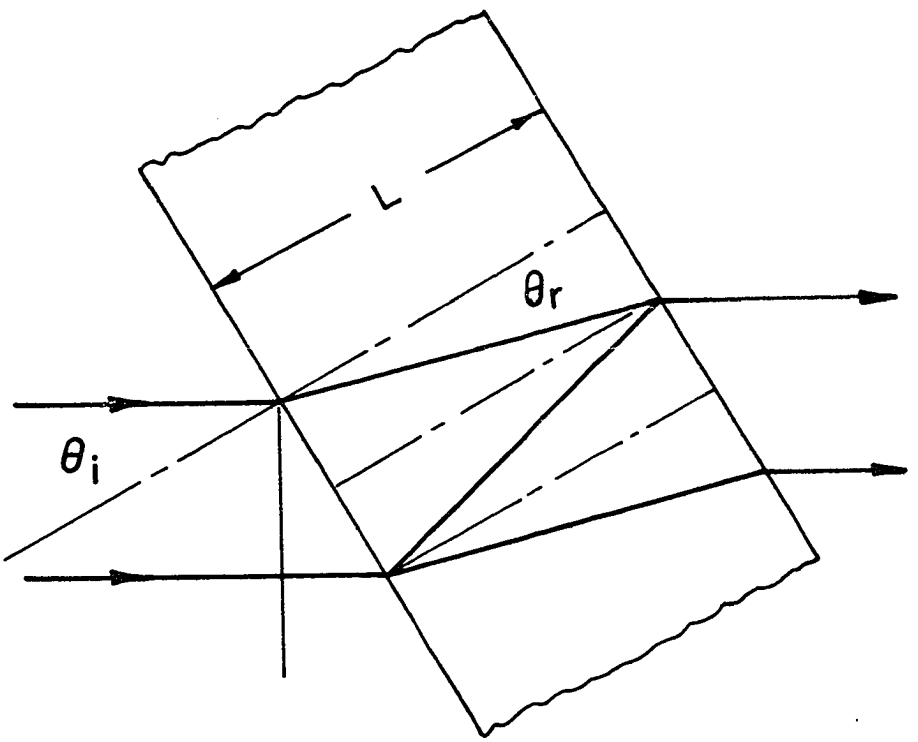

Figure 7. Optical path through a thin section.

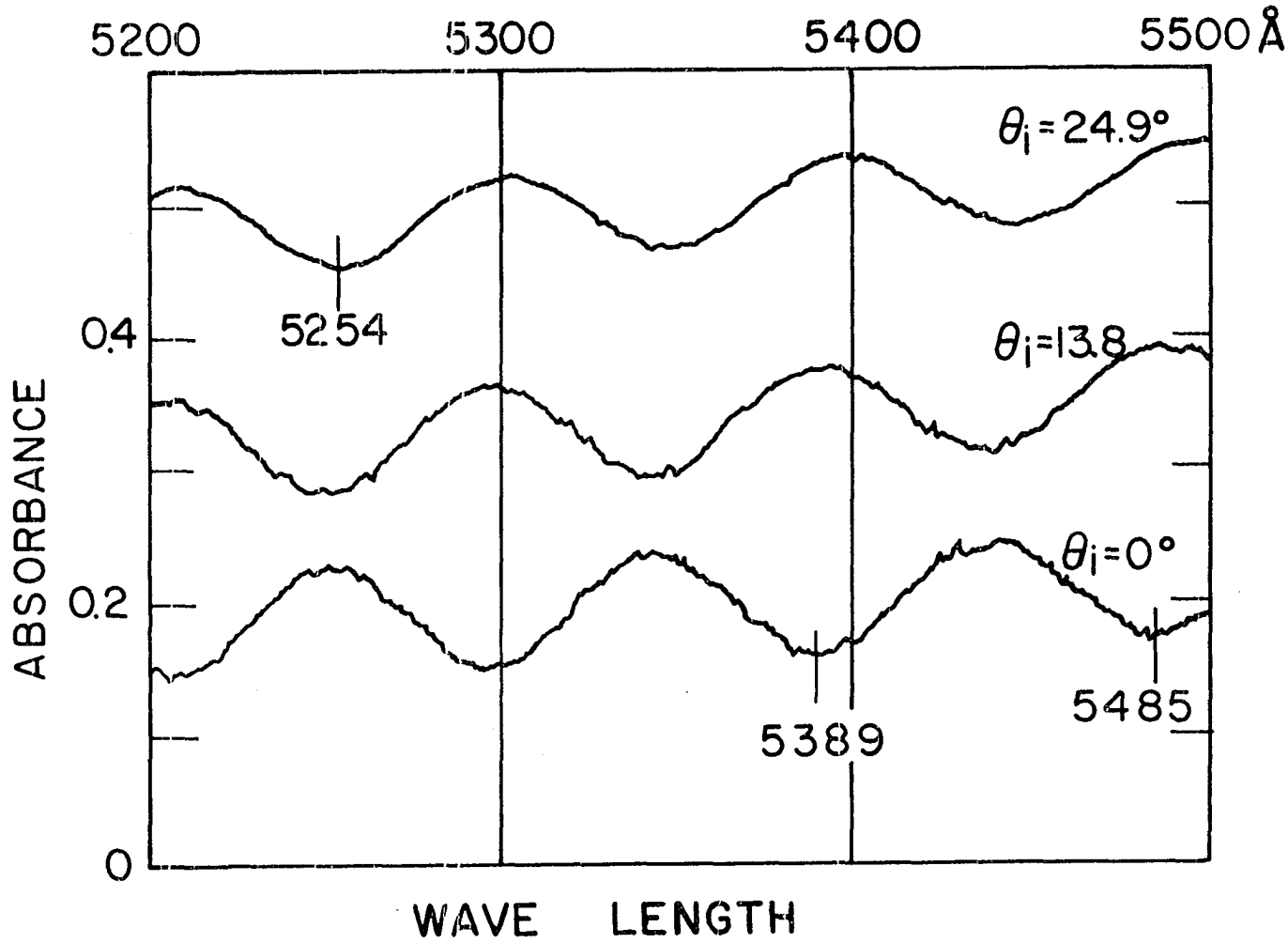

Figure 8. Recording of the absorbance for a-polarization over a limited wave length region with different angles of incidence. The spectra are for Magnus' green salt.

From equation 5 the limit was determined rather accurately by a linear least-squares and it would be equal to N if the dispersion, $(dn/d\bar{\nu})_N$, were zero. However, it was found that the last term in equation 5 was sometimes greater than 1 so N was not clearly designated without a value for the dispersion.

Equations 2 through 5 applied to a crystal whose face was perpendicular to the entering light ray. To determine the appropriate value of N unambiguously, the experiments were extended to include "tilted" crystal data. For uniaxial crystals, such as MGS, K_2PdCl_4 and K_2PdBr_4, the light ray entered a face containing the optic axis. It was possible to "tilt" or rotate the crystal in the beam about the optic axis. For example in Figure 8, a rotation through an angle θ_i resulted in a shift of the interference minimum at 5389Å to shorter wave lengths in tilts of 13.8 and 24.9 degrees. Under these conditions for a uniaxial crystal, Snell's law applied independently for both polarizations or $n = \sin \theta_i / \sin \theta_r$ (6). The angle of incident, θ_i, was known from experiment. The angle of refraction, θ_r, was shown (35) to be related to the phase delay of the doubly reflected wave by $\cos \theta_r = \delta_{\theta_i} / \delta_0$ (7) where δ_0 was the phase delay in the untilted crystal. The phase delay ratio was related to M for the zero and tilted scans by $\delta_{\theta_i} / \delta_0 = M_{\theta_i} / M_0$. (8)

It was possible to obtain satisfactory interference waves for incident angle rotations about the optic axis, $\theta_i = \pm 25$

to 30°. Calculation of the refractive index required that N, m_{θ_i} and m_0 be known at $\bar{\nu}_M$. For tilts of $\pm\theta_i$, the values of m_{θ_i} at minima and maxima were used to assign M_{θ_i} values in the tilted scans. The values of m_0 were calculated from the quadratic least-squares fit of $\bar{\nu}_M$ versus m for the zero tilt data. The indices of refraction were then calculated from the set of values of m_{θ_i} and m_0 and a number of trial integral values for N below the limit of $m\bar{\nu}_N/(\bar{\nu}_M-\bar{\nu}_N)$. The calculated sets of indices were then fitted by a linear least-squares giving n_N and the dispersion, $(\Delta n/\Delta\bar{\nu})$, over the region scanned. For K_2PdCl_4 and K_2PdBr_4 in the c-polarization, the values of N were selected which yielded the index of refraction in closest agreement with the value determined by the Becke line immersion method (34). Results for the compounds were summarized in Table 1.

Successive values of N produced changes of about 0.016 in the refractive index. Crystal thicknesses were calculated from the values of N, $\bar{\nu}_N$ and n_N in equation 2. As a test for consistency in the data, the values of n_N and $(dn/d\bar{\nu})_N$ were substituted back into equation 5 in order to generate a new value for N. In the c-polarization of K_2PdCl_4, the new N value from equation 5 was 39.0 in exact agreement with the previous value. For K_2PdCl_4, n_c was 1.541 at $\bar{\nu}_N$ = 18,020 cm^{-1}. In K_2PdBr_4 in c-polarization, the new N was 51.3 in comparison to the previous value of 50. This

Table 1. Summation of refractive index calculations

	Polariz.	$\bar{\nu}_N$ cm^{-1}	$\lim_{m\to 0} \frac{m\bar{\nu}_0}{\bar{\nu}_M - \bar{\nu}_N}$	n_N	$(dn/d\bar{\nu})_N$ 10^{-6} cm	N	n Na-D	L 10^{-4} cm
K_2PdCl_4	c	18,020	40.4	1.541	3.0	39	1.5389[a]	7.0
	a	17,310	45.0	1.69	13	40	1.68	
K_2PdBr_4	c	17,700	51.3	1.579	1.8	50	1.5808[a]	8.9
	a	16,380	60.1	1.79	20	51	1.749	
MGS	c	18,790		2.14[b]	10	65		
	a	18,550	57.3	1.87	1.96	56	1.864	8.09

[a]Determination of Becke line immersion method.

[b]An estimated value.

discrepancy probably reflected the uncertainty in the indicated dispersion; it did appear that the uncertainty in N and therefore in the thickness was probably no greater than ±1-2%.

In the a-polarization the refractive indices were not obtained from the Becke line method. Consistency tests were continued for n and $(dn/d\bar{\nu})_N$ until the values of N from equation 5 gave the closest agreement with the trial integral values. In Table 1 the indicated values of n_a were consistent with the qualitative observation of the Becke line. The higher dispersion in the a-polarization resulted from the proximity of strong absorption bands to $\bar{\nu}_N$; this method appeared accurate to within ±0.01 for the index of refraction. For K_2PdCl_4, n_a was 1.69 at 17,310 cm^{-1}; and for K_2PdBr_4, n_a was 1.749 at 16,380 cm^{-1}.

Interferometic determination of the refractive index for MGS was attempted for use in calculating crystal thicknesses. With 0, +24.03 and -24.87 degree tilts in a-polarization, consistency between the trial and calculated values of N were obtained for: $\bar{\nu}_N$ = 18,546 cm^{-1}, N = 56, $\lim_{m\to 0} \frac{m\bar{\nu}_N}{\bar{\nu}_M - \bar{\nu}_N}$ = 57.3, $(dn/d\bar{\nu})$ = 1.96 x 10^{-6} cm^{-1}, and n_a = 1.867. Using these data, n_a was 1.864 at the Na-D line. These parameters gave a calculated crystal thickness of 8.09 μ for a standard crystal. The region for recording absorbance waves was smaller in the c-polarization. A relation was set up between $n_c = N/2\bar{\nu}_N L$ (9) and $n_M = (N+m)/2\bar{\nu}_M L)$ (10) in order

to estimate a consistent value for n_c. Attempts were made to calculate N from several values of M or (N+m) and $\bar{\nu}_M$ using $\bar{\nu}_N$ = 18,790 cm^{-1} from the zero scan. The dispersion was negative when $N \geq 72$, so smaller values were tried. When N=70, n_c=2.304 and the dispersion was 2.3 x 10^{-6} cm which was close to the dispersion in a-polarization. In K_2PdCl_4 and K_2PdBr_4, the dispersion was greater in a-polarization, the direction of higher absorption. When N was decreased to 65, $n_{\bar{\nu}}$ = 2.14 and the dispersion was 1 x 10^{-5} cm. At this time, the value of n_c cannot be specified more exactly. These calculations were in agreement with the observation that $n_c > n_a > 1.74$ made by Cox et al. (36).

Thicknesses of other crystals were determined from the absorption spectrum at 300°K. Generally, a crystal's absorption was compared to that of the standard crystal of known thickness. Comparisons were made in both polarizations and they served as an adequate estimate of crystal thickness. Molar absorptivities could then be calculated.

Solution spectra were recorded using the Cary 14 spectrophotometer. Standard solutions of the palladium salts were prepared by dissolving the carefully weighed compound in solvents containing 2M NaBr or NaCl. Although bromide absorbs beyond 43,000 cm^{-1}, recording the spectra of $PdBr_4^{-2}$ in pure water was impractical because aquation occurred too rapidly (37). The spectrum of $PdBr_4^{-2}$ recorded from 25,000 to 44,000 cm^{-1} was obtained with 0.42 M KBr in order to minimize

bromide absorption. Components of the spectrum were resolved as log-normals by a least-squares program, LOGFIT (38). Solution extinction coefficients and oscillator strengths were from the components determined by LOGFIT and not the actual tracing.

III. RESULTS AND DISCUSSION

A. Tetraammineplatinum(II) Tetrachloroplatinate(II)

Magnus (39) first reported the action of ammonia on platinous chloride which resulted in a green compound now known as Magnus' green salt, MGS. The deep green color of tetraammineplatinum(II) tetrachloroplatinate(II) was the subject of considerable interest since solutions of the cation were colorless and solutions of the anion were red. Miller (40) showed that the deep green color was due to a "window" in the vicinity of 20,000 cm^{-1}. Cox, Pinkard, Wardlaw and Preston (36) showed that the tetragonal crystals of MGS contained alternate square-planar ions stacked in chains along the c-axis. Atoji, Richardson and Rundle (41) determined that $[Pt(NH_3)_4][PtCl_4]$ crystallized in the D_{4h}^6-P $4/m$ nc space group with two molecules per unit cell. As shown in Figure 9, the distance between planes was 3.24Å and the bonds in adjacent ions were staggered 28°. A single crystal with an hkO face was strongly dichroic in visible light. For light polarized along the chain or c-direction, a crystal appeared dark green in color. With light polarized in the plane or a-direction, a crystal was pale yellow in color.

Miller (40) reported the reflectance spectrum of MGS and attributed the green color to possible metal-metal interactions along the chain direction. Day, Orchard, Thompson and Williams (15) reported the room temperature polarized

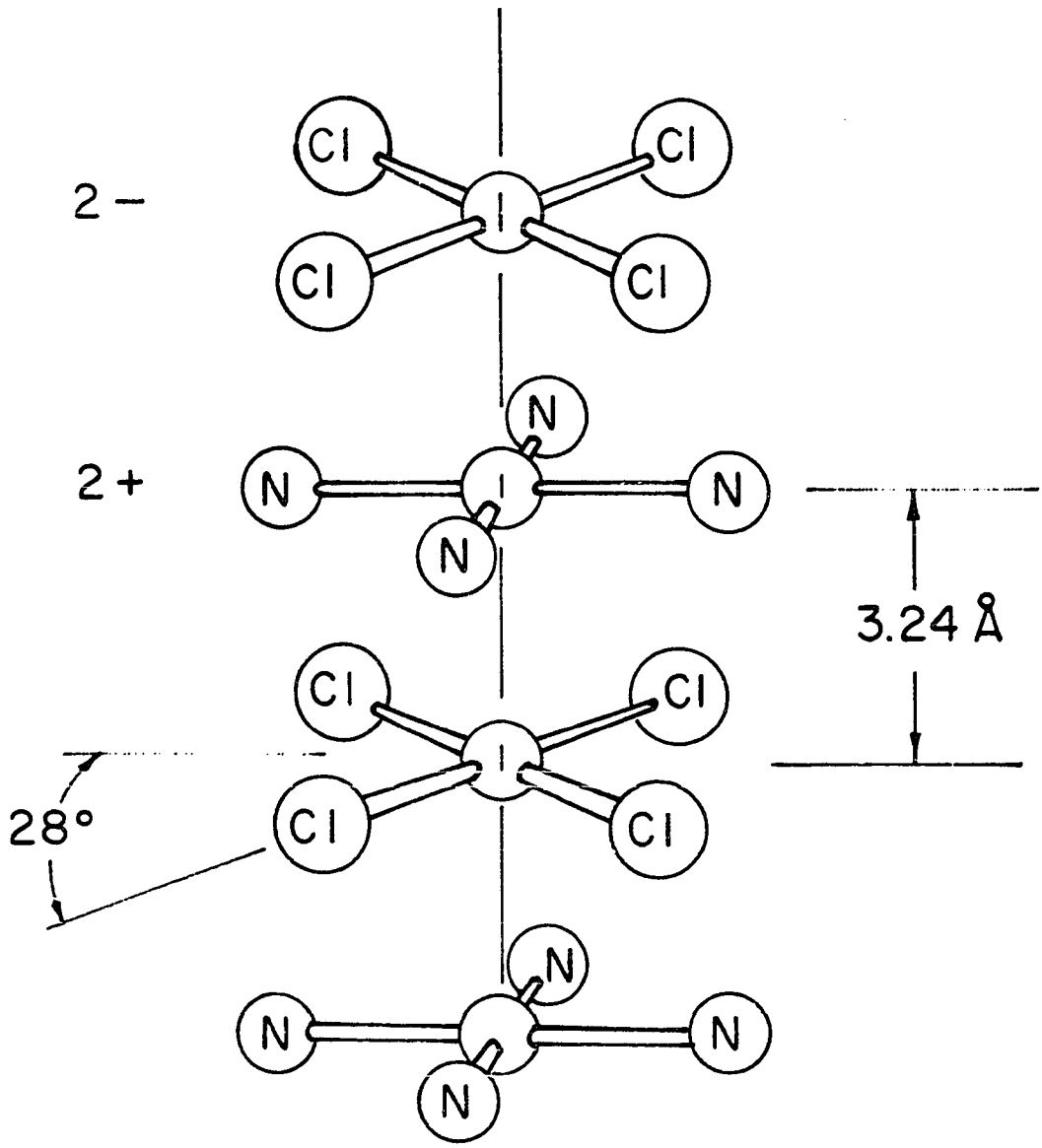

Figure 9. Alternate stacking of ions in Magnus' green salt.

spectra from 14,000 to 32,000 cm^{-1} for very tiny, single crystals. Their spectrophotometer utilized microscope condensing lenses to focus the beam on the crystal. Their investigations were supplemented by Anex, Ross and Hedgecock (42) who obtained polarized, single crystal, spectular reflectance data. In earlier studies, an intrinsic band model was proposed (15,40,43) to account for the different spectra obtained for the homologous series of complexes: $[PtA_4][PtCl_4]$ where A = NH_3, CH_3NH_2, $C_2H_5NH_2$. Interrante and Bundy (44) reported studies on the dependence of physical properties upon structural parameters. High pressure techniques were used to establish the relationship. With increasing pressure which decreased the Pt-Pt distance, the lowest energy visible absorption band was shifted to lower energy (44). Similar spectral studies for the alkylamine derivatives were reported (45).

In order to evaluate the structure-property relationship in MGS, Messmer and Interrante (46) reported a simple band theory calculation using an extended Hückel approach for MGS. Molecular orbital calculations were carried out on the individual constituent ions $Pt(NH_3)_4^{2+}$ and $PtCl_4^{2-}$, and then for the ion pair $[Pt(NH_3)_4PtCl_4]$. Their results for $PtCl_4^{2-}$ were essentially identical with those reported by Cotton and Harris (9). Results for $Pt(NH_3)_4^{2+}$ were consistent with chemical intuition and experiment (5,47). The difference in relative σ and π donor-acceptor properties of the Cl^- and NH_3

ligands was reflected in the significantly larger $b_{1g}(d_{x^2-y^2})$-$b_{2g}(d_{xy})$ orbital separation in $Pt(NH_3)_4^{2+}$ than in $PtCl_4^{2-}$. This was expected in view of Cl^- position in the spectrochemical series. The d-orbital ordering remained the same as that proposed by Chatt et al. (5).

The one-electron molecular orbital energy diagram for MGS was not significantly different than the diagrams for the individual ions. Using a Milliken population analysis, Messmer and Interrante (46) calculated the electron density in the bonding region between any two orbitals. In the ion pair case, the calculations indicated a net Pt-Pt bond order of 0.039 for which 0.038 was due to σ-bond interactions of $6p_z$-$5d_{z^2}$ and some 6s-$6p_z$ types. Interactions involving π-bonding accounted for 0.001 of the bond order and involved the $p_{x,y}$ and $d_{xz,yz}$ orbitals on the Pt atoms. The net Pt-Pt bond order (46) of 0.039 was not suggestive of appreciable metal-metal bonding in MGS. These calculations refuted Miller's claims for strong Pt-Pt bonding (40).

In order to simulate the linear chains in the MGS solid, they extended the calculations to include hypothetical chains of square-planar ions. Polymeric combinations of ions were considered. They obtained essentially the same Pt-Pt bond order for the polymeric case as in the ion pair. It was shown (43) that there were spectral differences within the homologous series. Since there was a correlation between

the color and the Pt-Pt distance (48), Messmer and Interrante varied intermolecular distances in their calculations. They found that interionic orbital interactions were negligible at a Pt-Pt separation of more than 4.0Å.

Since $Pt(NH_3)_4Cl_2 \cdot H_2O$ contained the $Pt(NH_3)_4^{2+}$ ion and was colorless (47), investigators concentrated on the $PtCl_4^{2-}$ ion as the significant spectral species. Intensities for the absorption of $PtCl_4^{2-}$ in red crystals of K_2PtCl_4 (17) were strongly temperature dependent as was the case for Cs_2PtCl_4 in Cs_2ZrCl_6 (21). For $PtCl_4^{2-}$ the lower energy transitions were vibronic in character. The corresponding polarized spectra of $PtenCl_2$ crystals contained weak but dipole-allowed transitions (23). These transitions were polarized normal to the chain direction and were attributed to unusual ionic exciton states for crystals of $PtenCl_2$. In $PtenCl_2$ the molecules were separated by 3.39Å (49) compared to 3.24Å in MGS. The possibility of electron transfers in MGS was suggested by Martin (1). The striking dichroism and closer stacking of the square-planar units in MGS suggested strong crystal interactions were operative. The present work was undertaken to study the temperature dependence of the crystal spectra.

Spectra were obtained from 16,700 to 32,000 cm^{-1} at 298°K and from 22,000 to 31,000 cm^{-1} at 15°K in a-polarization. Low intensity precluded reporting below 22,000 cm^{-1} at 15°K.

The three arrows represented intense transitions observed for K_2PtCl_4 in the x,y-polarization. In c-polarization the maximum which Day et al. placed at 16,500 cm^{-1} was not recorded due to instrumental limitations; however, the spectrum was recorded from 17,000 to 26,000 cm^{-1} at 298°K. The waves recorded in regions of low absorption were due to interference; vibrational structure was not observed in the recorded spectra. The absorption bands resolved from the spectra in Figure 10 were listed in Table 2.

Day et al. (15) reported a peak maximum at 16,500 cm^{-1} ($\varepsilon \approx 140$ $cm^{-1}M^{-1}$) in c-polarization. Although this maximum was not recorded, the band clearly decreased in intensity at 15°K. The absorption decreased so much that interference waves were observed in this region. Therefore, this band was attributed to a vibronic excitation. The spectrum was scanned as far as 26,000 cm^{-1} where the absorbancy increased continuously to a value greater than 700 $cm^{-1}M^{-1}$. Day et al. reported a maximum of 300 $cm^{-1}M^{-1}$ at 25,000 cm^{-1} followed by a valley at 28,000 cm^{-1}. The peak and valley were directly over a peak and valley in a-polarization; these features reported by Day et al. were not duplicated in this study. Apparently, their phototube intercepted low intensity light, which probably arose from the convergence of light by the condensing microscope lens used in their optical system (15). This would have introduced a c-polarization component. Possibly crystalline surface defects also scattered light with some

Figure 10. Polarized crystal spectrum for Magnus' Green Salt. For a-polarization the light entered a (001) face of a crystal 10.6 μ thick and the spectrum was recorded without polarizer. For c-polarization the light entered a (hk0) face of a crystal which was 8.1 μ thick.

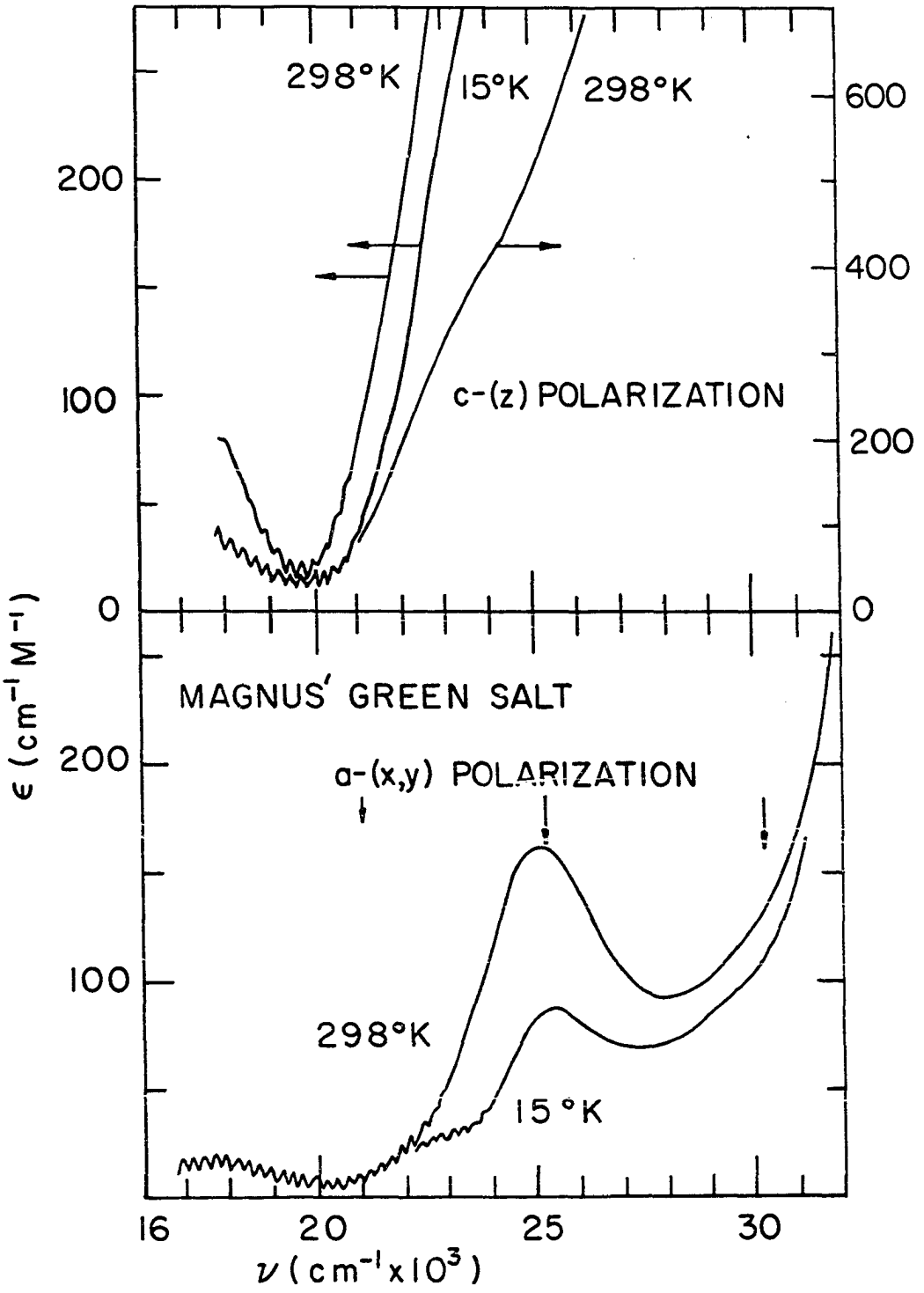
298°K
15°K
298°K
600
200
400
100
c-(z) POLARIZATION
200
0
0
MAGNUS' GREEN SALT
ε (cm⁻¹ M⁻¹)
200
a-(x,y) POLARIZATION
100
298°K
15 °K
16
20
25
30
ν (cm⁻¹ x 10³)

depolarization. These factors may have contributed to the intensity. Hence, it was concluded that the maximum they reported (15) at 25,000 cm^{-1} and the valley at 28,000 cm^{-1} in the c-polarization were spurious.

Anex, Ross and Hedgecock (42) reported an intense band at 34,500 cm^{-1} for light with z-polarization in the specular reflectance spectrum of MGS. Since the symmetry forbidden $\sigma^{*}\leftarrow d$ transitions borrow intensity from adjacent allowed transitions, their intensity should be higher. At 298°K the band at 16,500 cm^{-1} (ε = 80 $cm^{-1}M^{-1}$) is assigned to the $^{3}A_{2g}\leftarrow{}^{1}A_{1g}(b_{1g}-\sigma^{*}\leftarrow b_{2g}-d_{xy})$ and the $^{3}E_{g}\leftarrow{}^{1}A_{1g}(b_{1g}-\sigma^{*}\leftarrow e_{g}-d_{xz,yz})$ transitions in agreement with Day *et al.* (15). These states were observed at 20,200 cm^{-1} (ε = 20 $cm^{-1}M^{-1}$) in K_2PtCl_4 and were red shifted about 4,100 cm^{-1} in MGS. The 16,500 cm^{-1} band was red shifted *ca.* 2,000 cm^{-1} with 16.5 kbars of pressure representing a Pt-Pt distance of *ca.* 3.14Å (44). There was an intensity increase for these transitions in MGS. There were no other bands resolved in the z-polarization except for possibly an uncertain shoulder at 23,000 or 24,000 cm^{-1}.

In the a-polarization in the vicinity of 17,000 cm^{-1}, the absorption was so low for these thin crystals that little can be reported about any bands in this region. There was a peak with a maximum at 25,000 cm^{-1} with a molar absorptivity of 160 $cm^{-1}M^{-1}$ in good agreement with that reported by Day

et al. (15). This maximum appeared to lie on the tail of a much more intense band above 32,000 cm^{-1}. The valley at ca. 28,000 cm^{-1} was perhaps not as deep as in the spectrum of Day et al. When the crystal was cooled, the intensity dropped off considerably and the maximum shifted to 25,200 cm^{-1}, as shown in Figure 10. Hence, it was inferred that this band was excited vibronicly.

At liquid helium temperatures, a shoulder was evident on the low energy side of the band. The absorption at 15°K was resolved into gaussian components with a weak band at 23,000 cm^{-1} (ε = 20 $cm^{-1}M^{-1}$) and a major band at 25,200 cm^{-1} (ε = 65 $cm^{-1}M^{-1}$). The oscillator strengths were included in Table 2. There was some uncertainty in these oscillator strengths because the tail of a higher energy absorption contributed considerably to the intensity in this region. Three transitions for K_2PtCl_4 were shown by the arrows in Figure 10. These transitions were reported by Martin, Tucker and Kassman (17) as $\sigma^* \leftarrow d$ transitions. The $^1A_{2g}$ and ^1E_g states were reported at 26,300 and 29,200 cm^{-1}, respectively. In MGS there is a single maximum at 25,200 cm^{-1} which was believed to include both bands. Thus in x,y-polarization, the $^1A_{2g} \leftarrow {}^1A_{1g}$ ($b_{1g}-\sigma^* \leftarrow b_{2g}-d_{xy}$) transition has been red shifted only ca. 1,100 cm^{-1} whereas the $^1E_g \leftarrow {}^1A_{1g}$($b_{1g}-\sigma^* \leftarrow e_g-d_{xz,yz}$) transition has been shifted ca. 4,200 cm^{-1}.

Table 2. Transitions in $Pt(NH_3)_4PtCl_4$, MGS[a]

$\bar{\nu}$-cm^{-1}	ε_{max}-$cm^{-1}M^{-1}$	Polarization	Osc. Strength f x 10^4	Red Shift $\Delta\bar{\nu}$ cm^{-1}	Transition Assignment Ground State - $^1A_{1g}$
16,500[b]	ca. 50[c] (110)	z	-	-4,100	$^3A_{2g}$, $^3E_g \leftarrow {}^1A_{1g}$
23,000	20	xy	2 (-)		$^3B_{1g} \leftarrow {}^1A_{1g}$
25,200	65 (140)	xy	7.3 (20)	-1,100, -4,000	$^1A_{2g}$, $^1E_g \leftarrow {}^1A_{1g}$
34,500[d]		z	Intense	-16,000 to -20,000	$^1A_{2u} \leftarrow {}^1A_g$ (a_{2u}-$p_z \leftarrow a_{1g}$-d_{z^2})

[a]Values of ε and f without parentheses are for 15°K. Values in parentheses are for 300°K.

[b]From reference (15).

[c]By extrapolation.

[d]From reference (42).

There was a weak transition at 23,000 cm^{-1} in a-polarization which was presumably a spin forbidden transition. This transition was very close in energy to the $^3B_{1g} \leftarrow {}^1A_{1g}$ (b_{1g}-$\sigma^* \leftarrow a_{1g}$-$d_{z^2}$) transition observed in K_2PtCl_4 at 24,000 cm^{-1} (ε = 7 $cm^{-1}M^{-1}$). In K_2PtCl_4 the 24,000 cm^{-1} band was assigned in the D_4' double rotational group to the $E_1'(\Gamma_5)$ component of the $^3B_{1g}$ state; whereas, the $B_2'(\Gamma_4)$ component was some 3,000 cm^{-1} higher in energy. The 23,000 cm^{-1} band in MGS may be assigned to the $B_2'(\Gamma_4)$ component of the $^3B_{1g}$ state. It seems unlikely that it is the $E_1'(\Gamma_5)$ component in view of the high spin-orbit coupling of Pt and the close proximity to the transition at 25,000 cm^{-1}.

Isci and Mason (47) reported the MCD spectrum for the $Pt(NH_3)_4{}^{2+}$ cation in aqueous and acetonitrile solutions. The lowest energy band at 34,750 cm^{-1} was assigned to the spin-forbidden $^3A_{2g}$ and $^3E_g \leftarrow {}^1A_{1g}$ transitions on the basis of the unresolved, broad B terms observed in the MCD spectrum (47). Shoulders observed at 41,500 and 45,500 cm^{-1} were assigned to the $^1A_{2g} \leftarrow {}^1A_{1g}$ and $^1E_g \leftarrow {}^1A_{1g}$ transitions. In the MCD spectrum a definite A term was observed for the intense band at 50,950 cm^{-1}. Isci and Mason assign this band to the $^1E_u \leftarrow {}^1A_{1g}$($a_{2u}$-$p_z \leftarrow e_g$-$d_{xz,yz}$) transition. In MGS, it was likely that the transitions for $Pt(NH_3)_4{}^{2+}$ were shifted in energy. Since the transitions in $Pt(NH_3)_4{}^{2+}$ are generally higher in energy than the corresponding transitions in $PtCl_4{}^{2-}$, it was

assumed that the $Pt(NH_3)_4^{2+}$ transitions in MGS crystals were beyond the experimentally accessible region.

In a crystal such as $Pt(NH_3)_4PtCl_4$ with two molecules per primitive cell, it is possible to have Davydov splitting of each excited state into two crystal states. In this case one transition has zero intensity due to the parallel alignment of the molecular axes and the uniform separation along the chain. Only one transition is seen. In a simple treatment, the crystal is viewed as an aggregate of non-interacting oriented molecules in a rigid lattice. This type of treatment has been employed by Martin and coworkers for $PtenCl_2$ (23) and $PtenBr_2$ (24), and can be applied for MGS.

In analogy with $PtenCl_2$ and $PtenBr_2$ crystal effects can account for the apparent red shift in the vibronic excitations in MGS. For $\sigma^* \leftarrow d$ transitions the individual spacial extent of the d-orbitals must be considered. The $d_{x^2-y^2}$ orbital is concentrated in the bonding plane. The d_{xy} orbital is located in the $PtCl_4^{2-}$ plane whereas the d_{xz} and d_{yz} orbitals are π-antibonding and are out of the plane. If the red shift results from the repulsion of intermolecular electrons, the most strongly shifted transitions should be those involving some orbital which is out of the anion plane. For example, the ^1E_g state was shifted 4,000 cm^{-1} compared to the 1,100 cm^{-1} shift for the $^1A_{2g}$ state. The red shift may represent the coulombic interactions among neighboring ions in columnar

arrays. Crystal field forces are closely related to the Pt-Pt distance as is shown by the red shift in the ^3E_g to $^3A_{2g}$ states at higher pressures (44).

Assuming cyclical boundary conditions for MGS, the transition energy from the ground state, ψ_{Gr} to the excited state, ψ_{Ex}, is:

$$\bar{\nu}(\psi_{Ex} \leftarrow \psi_{Gr}) = \bar{\nu}_0 + D + I \qquad (11)$$

The transition energy for the free ion in the gaseous state is represented by $\bar{\nu}_0$. The D in equation 11 represents the difference in the van der Waal's energy between the ground and excited states. For $PtenCl_2$ and $PtenBr_2$, Martin and coworkers assumed the D term was negative which results in lowering the transition energy, $\bar{\nu}$. The I represents exchange terms and these are the type of interactions which lead to Davydov splitting in the exciton states of crystals. For example, in $PtenCl_2$ a z-polarized band at 37,500 cm^{-1} was shifted at least from 46,000-53,000 cm^{-1} region of the solution spectrum (23). The I term was estimated for that case by the summation of interactions between transition dipoles to be ca. -6,000 cm^{-1} and did not totally account for the shift (23). Therefore, the D term as well as solvent effects in the solution spectrum were suggested as contributing to the observed shift (23,32). Martin and coworkers concluded for $PtenCl_2$ that a z-polarized band for a columnar stack will be shifted to lower energy while an x or y-polarized band will be

shifted to higher energies (23,32). The study of $PtenBr_2$ presented a similar case for Frenkel excitons in molecular crystals (24,33).

It appeared that coulombic interactions affected intra-ionic transitions for the $PtCl_4^{2-}$ ion in MGS. Interionic electron transfers to produce ionic exciton states were not observed for MGS in the spectral regions investigated. The transition at 34,500 cm^{-1} reported by Anex et al. (42) was very intense and was z-polarized. That this exciton in MGS was subject to extensive crystal effects in the columnar arrays is evident from anion cation separation characteristic of MGS-type compounds. The 34,500 cm^{-1} band is assigned to the $^1A_{2u} \leftarrow {}^1A_{1g}(a_{2u}\text{-}p_z \leftarrow a_{1g}\text{-}d_{z^2})$ transition which has been red shifted some 16,000 to 20,000 cm^{-1} from the free ion energies. The terms in equation 11 can estimate the origins for the red shift.

As in $PtenCl_2$, the D term for MGS is assumed to be negative.

Possibly the free ion energy, $\bar{\nu}_0$ can be estimated from the energies of the $^1A_{2u}$ states in the constituent ions of MGS. In $Pt(NH_3)_4Cl_2 \cdot H_2O$ an intense band near 48,000 cm^{-1} was reported as a p←d transition by Chatt et al. (5). Anex and coworkers (42) have claimed that the intense band at ca. 51,200 cm^{-1} in aqueous solutions of $Pt(NH_3)_4^{2+}$ corresponded to the same transition as was observed at 46,000 cm^{-1} for

K_2PtCl_4. Anex and Takeudhi (22) reported a very intense, z-polarized band at 46,000 cm^{-1} for crystals of K_2PtCl_4. A very intense band was reported (50) for K_2PtCl_4 in acetonitrile solution at 54,200 cm^{-1} (ϵ = 50,400 $cm^{-1}M^{-1}$). These intense bands are p←d transitions; in $Pt(NH_3)_4^{2+}$ and $PtCl_4^{2-}$ the $^1A_{2u}$ states lie close in energy.

The components of the I term in equation 11 for a columnar stack can be estimated in terms of the transition moment $\hat{R}$ as:

$$I_{N,M} = e^2r^{-3}(\hat{R}_{x,N}\hat{R}_{x,M} + \hat{R}_{y,N}\hat{R}_{y,M} - 2\hat{R}_{z,N}\hat{R}_{z,M}) \qquad (12)$$

In equation 12 N and M refer to different atoms, r is the separation, and $\hat{R}_x$, $\hat{R}_y$ and $\hat{R}_z$ are the transition moments. The contribution $I_{N,M}$ is greater for z-polarized bands than for x,y-polarized bands. The I term in equation 11 will be large and negative, so the large, red shift in MGS for the $^1A_{2u}$ states is not unreasonable. The band at 34,500 cm^{-1} is an intraionic exciton for both ions in MGS (51).

B. Potassium Tetrachloropalladate(II)

Crystals of potassium tetrachloropalladate(II) were first prepared by Gutbier and Krell (52) in 1905. Dickinson (3) determined through X-ray diffraction that crystals of K_2PdCl_4 and K_2PtCl_4 were isomorphous. The tetragonal P4/mmm space group was confirmed for K_2PdCl_4 by later workers (53). The most recent study of its crystal spectra was reported by Francke and Moncuit (54).

The energy states and transition assignments for potassium tetrachloropalladate(II) have been discussed in terms of a series of one electron molecular orbitals. Basch and Gray (8) and later Katô (27) reported MO calculations for $PdCl_4^{-2}$. According to their computations, the ligand and metal orbitals were separated in energy. Tondello, DiSipio, DeMichelis and Oleari (55) reported semi-empirical SCF-MO-LCAO calculations which were claimed to evaluate transition energies by a configuration interaction procedure for the excited state. From the eigenvalues the energy ordering of the d-orbitals was $d_{z^2}<d_{xy}<d_{xz}=d_{yz}<d_{x^2-y^2}$ which was not representative of the known spectra (15,54).

Messmer, Interrante and Johnson (28) performed SCF-Xα-SW calculations for K_2PdCl_4. The ground state orbital energy levels were calculated using Johnson's (56) scattered wave (SW) approach to molecular orbital theory and their ordering of these levels has been reproduced qualitatively in Figure 11. The d-orbital ordering was consistent with the order proposed by Chatt et al. (5) for platinum(II) complexes. In Figure 11 the ordering was different from that proposed for $PdCl_4^{2-}$ by Basch and Gray or Katô. In particular the b_{2u}, a_{2g} and e_u orbitals, primarily of $L\pi$ character, were between the e_g-$d_{xz,yz}$ and a_{1g}-d_{z^2} orbitals. The orbital diagram in Figure 11 implies that $\sigma^*\leftarrow d$ and $\sigma^*\leftarrow L$ transitions would likely be close in energy. If the $\sigma^*\leftarrow L$ transitions were at lower energies than for the platinum(II) complexes, these transitions would be observable.

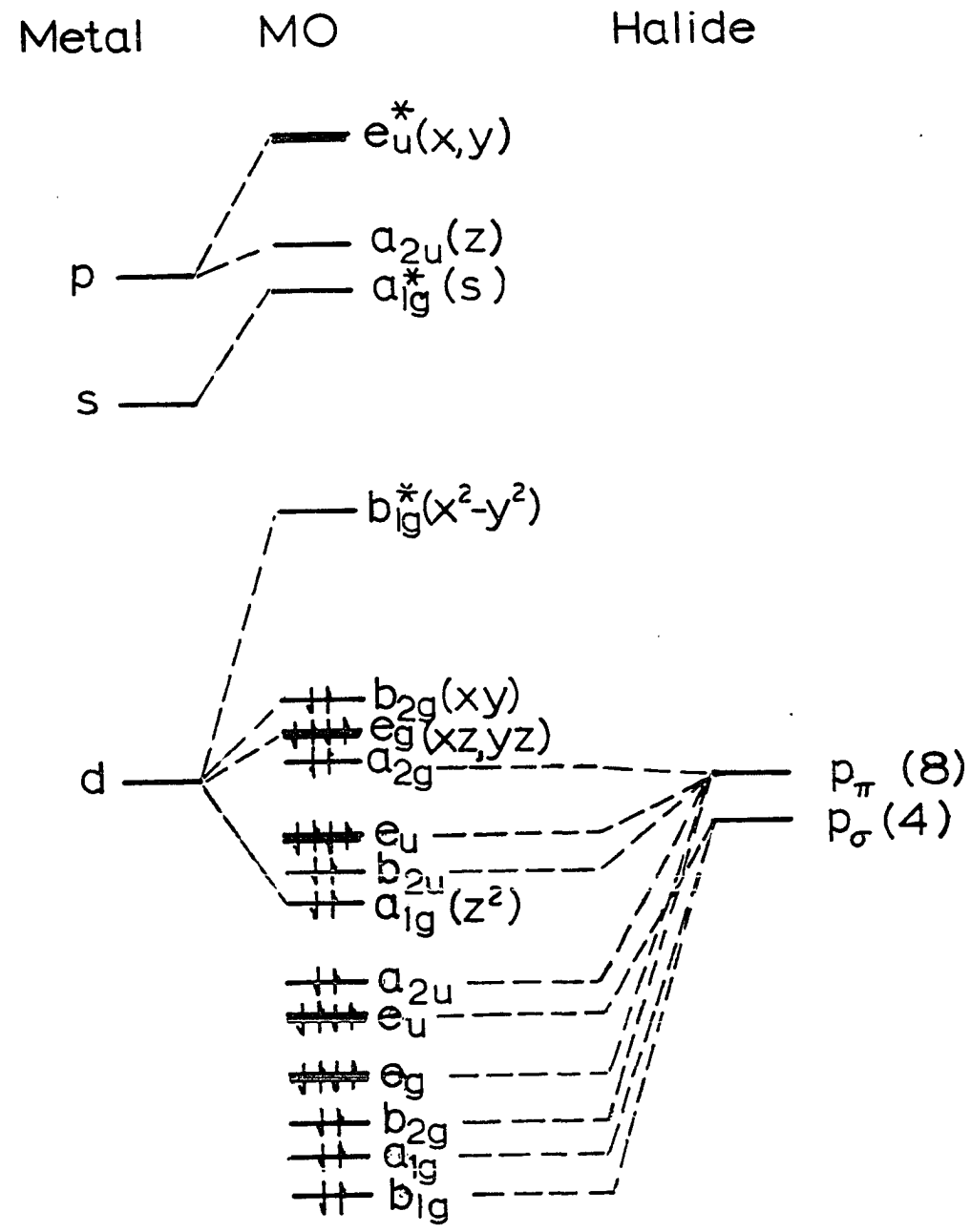

Figure 11. Molecular orbital diagram for palladium(II) complexes. Reproduced qualitatively from reference (28).

Hence, in this work the polarized crystal spectra were obtained in the visible and near ultraviolet regions at 300 and 15°K.

The visible and ultraviolet spectra of tetrachloropalladate(II) in various polar solvents were reported by Harris, Livingstone and Reece (57). In particular, Harris et al. reported spectra for K_2PdCl_4 in H_2O-1M $HClO_4$ and in nujol mulls. McCaffery and coworkers (18) reported the MCD spectrum of K_2PdCl_4 in 2M HCl. In the aqueous spectrum in Figure 12, the lowest energy maximum occurs at 21,000 cm^{-1} with a molar absorption of 162 $cm^{-1}M^{-1}$. An MCD-A term was observed at 21,100 cm^{-1} so a transition to a degenerate excited state was indicated for this region (18). The transition was presumably the $^1E_g \leftarrow {}^1A_{1g}(b_{1g}-\sigma^* \leftarrow e_g-d_{xz,yz})$.

At room temperature in the polarized crystal spectra, there were maxima at 21,200 cm^{-1} (ε_{max} = 250 $cm^{-1}M^{-1}$) in a-polarization and at 23,000 cm^{-1} (ε_{max} = 90 $cm^{-1}M^{-1}$) in c-polarization as shown in Figure 13. In a-polarization, vibrational fine structure was observed on the low energy side of the band with maximum at 21,700 cm^{-1}. The structure faded out on the high energy side of this band. The 21,700 cm^{-1} band was missing in the z-polarized spectrum. It was concluded from the selection rules that this band was the $^1A_{2g} \leftarrow {}^1A_{1g}(b_{1g}-\sigma^* \leftarrow b_{2g}-d_{xy})$ transition. The $^1E_g \leftarrow {}^1A_{1g}(b_{1g}-\sigma^* \leftarrow e_g-d_{xz,yz})$ transition was observed as a shoulder in the x,y-polarization at 23,200 cm^{-1} and as a peak at this same

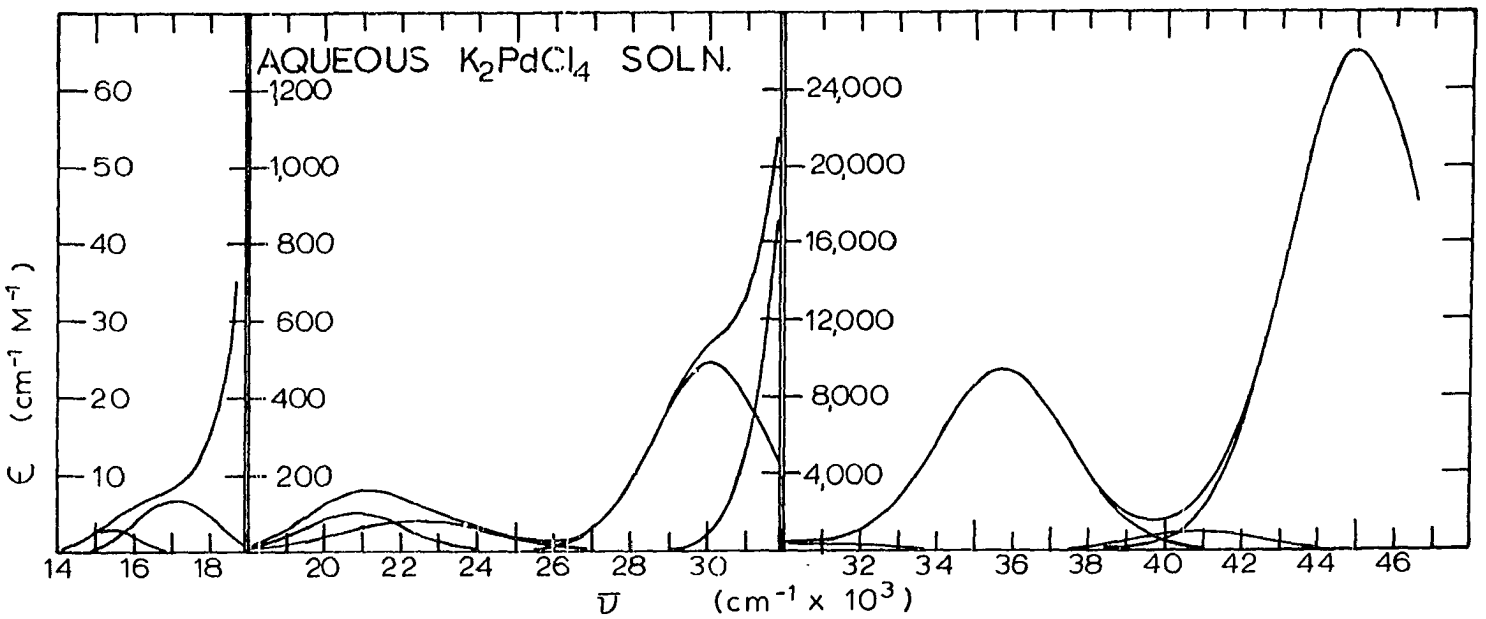

Figure 12. Aqueous spectrum of K_2PdCl_4 in 2M NaCl.

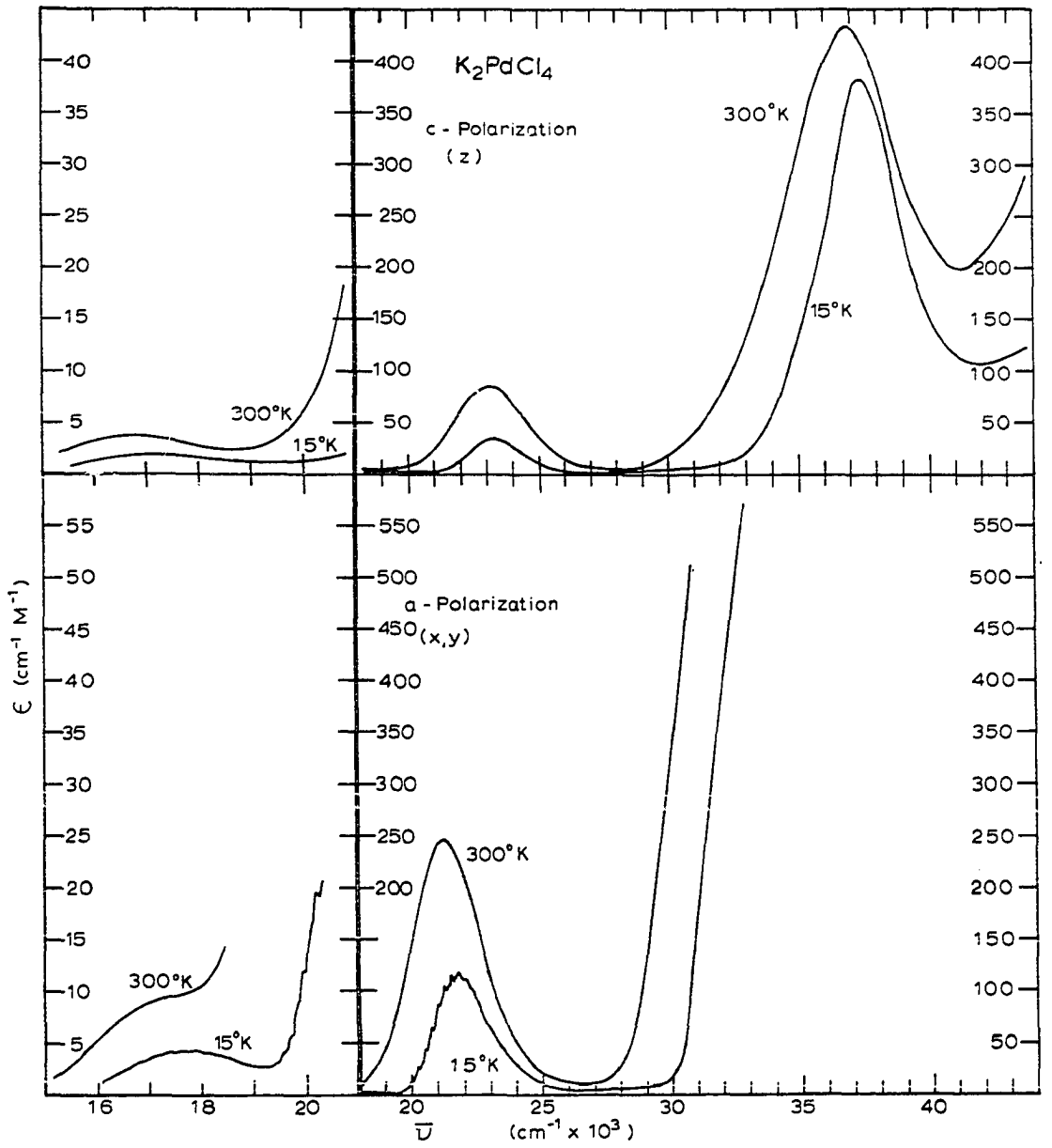

Figure 13. Polarized crystal spectra for K_2PdCl_4. From 16,000 to 20,000 cm^{-1} the crystal was 126 μ thick. From 18,000 to 29,000 cm^{-1} the crystal was 10.5 μ thick. Above 29,000 cm^{-1} the crystal was 3 μ thick.

energy in z-polarization. The $^1A_{2g}$ and ^1E_g bands were not as completely resolved in x,y-polarization as was the case for K_2PtCl_4 (17).

As for K_2PtCl_4, vibrational structure was associated with the $^1A_{2g} \leftarrow {}^1A_{1g}$ and not the $^1E_g \leftarrow {}^1A_{1g}$ transition (17). In K_2PdCl_4 the vibrational progressions consisted of 12 maxima and 9 poorly resolved shoulders; each shoulder was approximately 120 cm^{-1} below the maximum. The intensity of the $^1A_{2g} \leftarrow {}^1A_{1g}$ transition was due to asymmetries induced by vibrations of E_u symmetry. These vibrational perturbations removed the inversion center to give partial allowedness to this otherwise forbidden transition. The $PdCl_4^{2-}$ ion has two in-plane E_u molecular vibrations, namely - ν_6 primarily a stretching and ν_7 primarily a bending mode. The vibrational progressions were consistent with excitation of the maxima by ν_6 and the shoulders by ν_7. Since the fine structure was observed in an absorption spectrum, the structure was representative of the vibrational levels in the excited state. The energy separation between a maximum and its shoulder was 120 cm^{-1}. This separation represented the difference between ν_6 and ν_7. The observed difference of 120 cm^{-1} was reasonable in comparison to the ground state difference of 143 cm^{-1} (ν_6 = 336 cm^{-1}, ν_7 = 193 cm^{-1}) (58). Individual maxima and shoulder locations were tabulated in Table 3. The separation between successive maxima averaged 264 ± 10 cm^{-1}. This

Table 3. Vibrational structure resolved on the $^1A_{2g} \leftarrow {}^1A_{1g}$ transition for K_2PdCl_4 at 15°K

x,y-Polarization (cm^{-1})	
19430	20750
19570 sh	20890 sh
19680	21020
19800 sh	21160 sh
19450	21280
20100 sh	21422 sh
20210	21540
20360 sh	21810
20480	22070
20640 sh	22320

periodic separation can be viewed as excitation of the totally symmetric breathing vibration, ν_1. Again the 264 cm^{-1} value for ν_1 was reasonable with respect to the ground state value of 310 cm^{-1} reported from the Raman spectrum (58,59). The observed frequencies were less than the ground state values, as was expected (1).

The principle features below 25,000 cm^{-1} in the absorption spectra of K_2PdCl_4 were similar to the spectra reported by Francke and Moncuit (54). In agreement with Francke and Moncuit, the component in the x,y-polarization was centered at 21,000 cm^{-1} and not at 22,600 cm^{-1} as reported by Day et al. (15). The molar absorptivity was 245 $cm^{-1}M^{-1}$ as shown in Figure 12. The $^1A_{2g}$ and $^1E_g \leftarrow {}^1A_{1g}$ transitions were reported

(54) at 12°K with molar absorptivities of 25 and 23 $cm^{-1}M^{-1}$, respectively. These transitions had almost 1.5 times higher intensities than was reported by Francke and Moncuit. The location of the vibrational structure was comparable to that reported by Francke and Moncuit. However in thick crystals, the molar absorptivity agreed well with their values for the spin-forbidden bands below 20,000 cm^{-1} in both polarizations.

The absorption between 16,000 and 19,000 cm^{-1} in solution and in the crystals was presumably due to spin-forbidden $\sigma^* \leftarrow d$ transitions to the $^3A_{2g}$ and ^3E_g states. The component resolved using LOGFIT had an oscillator strength of ca. 10^{-5} which was much less than that obtained for the spin allowed bands centered at 21,700 cm^{-1}. Harris et al. (57) had reported that these transitions to triplet states were roughly one-half as intense as the singlets. The low intensity of these transitions to triplet states is consistent with the lower spin-orbit coupling of the palladium in comparison to platinum. Very faint vibrational structure appeared in the a-polarization at 15°K. Complete identification of the individual triplet states was not possible.

In the solution spectrum of K_2PdCl_4, there was a component resolved at 30,100 cm^{-1} with an absorptivity of 490 $cm^{-1}M^{-1}$. This component was obvious as a shoulder at 30,200 cm^{-1} (ε = 540 $cm^{-1}M^{-1}$) in the spectrum reported by McCaffery et al. (18). The MCD spectrum was not reported

from ca. 27,000 to 37,000 cm^{-1} and McCaffery et al. listed this shoulder without discussing it. The absorption in both polarizations for the crystal was very low in this region. It was concluded that this component was not due to $PdCl_4^{2-}$ but possibly to a minor solution species.

In thin crystals the absorption was low from 26,000 to 29,700 cm^{-1} in a-polarization and from 26,000 to 31,000 cm^{-1} in c-polarization. Francke and Moncuit (54) reported a very small but distinct peak at 28,500 cm^{-1} (ϵ = 5 $cm^{-1}M^{-1}$, 12°K) in a-polarization for a crystal 176 μ thick. In order to duplicate their report, spectra for a thick crystal were obtained as was shown in Figure 14. Close examination indicated no negative curvature which would identify a shoulder at 15°K in either polarization. In this region the molar absorptivity was only ca. 1-2 and no vibrational structure was observed. Absorption in this region was no more intense than for the spin-forbidden d←d transitions. The absorption minimum was asymmetric in x,y-polarization possibly due to the tail of a very intense band at higher energies. The spectral results showed that a very weak band could be present since the absorption was not zero; however, any transition assignment would be highly speculative. Assignments of the low energy bands have been summarized in Table 4.

Francke and Moncuit observed a shoulder near the upper limit of their scan in the z-polarization at ca. 33,000 cm^{-1}

Table 4. Spectral components resolved for K_2PdCl_4

$PdCl_4^{2-}$ Aqueous Spectrum at 300°K			K_2PdCl_4 Crystal Spectra at 15°K						Transition Assignments
			c-z Polarization			a-x,y Polarization			
$\bar{\nu}$, cm^{-1}	ε, $cm^{-1}M^{-1}$	Osc.Str.	$\bar{\nu}$, cm^{-1}	ε, $cm^{-1}M^{-1}$	Osc.Str.	$\bar{\nu}$, cm^{-1}	ε, $cm^{-1}M^{-1}$	Osc.Str.	
15,350	3	2.1×10^{-5}							
17,000	7	7.8×10^{-5}	17,000	1	1.2×10^{-5}				$^3A_{2g} \leftarrow {}^1A_{1g}(b_{1g}\text{-}\sigma^* \leftarrow b_{2g}\text{-}d_{xy})$
						17,700	3.0	3.3×10^{-5}	$^3E_g \leftarrow {}^1A_{1g}(b_{1g}\text{-}\sigma^* \leftarrow e_g\text{-}d_{xz,yz})$
20,820	100	1.4×10^{-3}				21,700	118	9.6×10^{-4}	$^1A_{2g} \leftarrow {}^1A_{1g}(b_{1g}\text{-}\sigma^* \leftarrow b_{2g}\text{-}d_{xy})$
22,440	78	1.75×10^{-3}	23,200	36	4.2×10^{-4}	23,200	30	4.8×10^{-4}	$^1E_g \leftarrow {}^1A_{1g}(b_{1g}\text{-}\sigma^* \leftarrow e_g\text{-}d_{xz,yz})$
30,100	490	7.7×10^{-3}	Not Present			Not Present			Not $PdCl_4^{2-}$
35,720	9,330	0.17				Intense Absorption			$^1E_u \leftarrow {}^1A_{1g}(b_{1g}\text{-}\sigma^* \leftarrow e_u\text{-}L\pi)$
			37,400	388	7.2×10^{-3}	Intense Absorption			$^1A_{2u} \leftarrow {}^1A_{1g}(b_{1g}\text{-}\sigma^* \leftarrow b_{2u}\text{-}L\pi)$
40,780	900	1.4×10^{-2}				Intense Absorption			
44,980	25,800	0.511				Intense Absorption			$^1E_u \leftarrow {}^1A_{1g}(b_{1g}\text{-}\sigma^* \leftarrow e_u\text{-}L\sigma)$

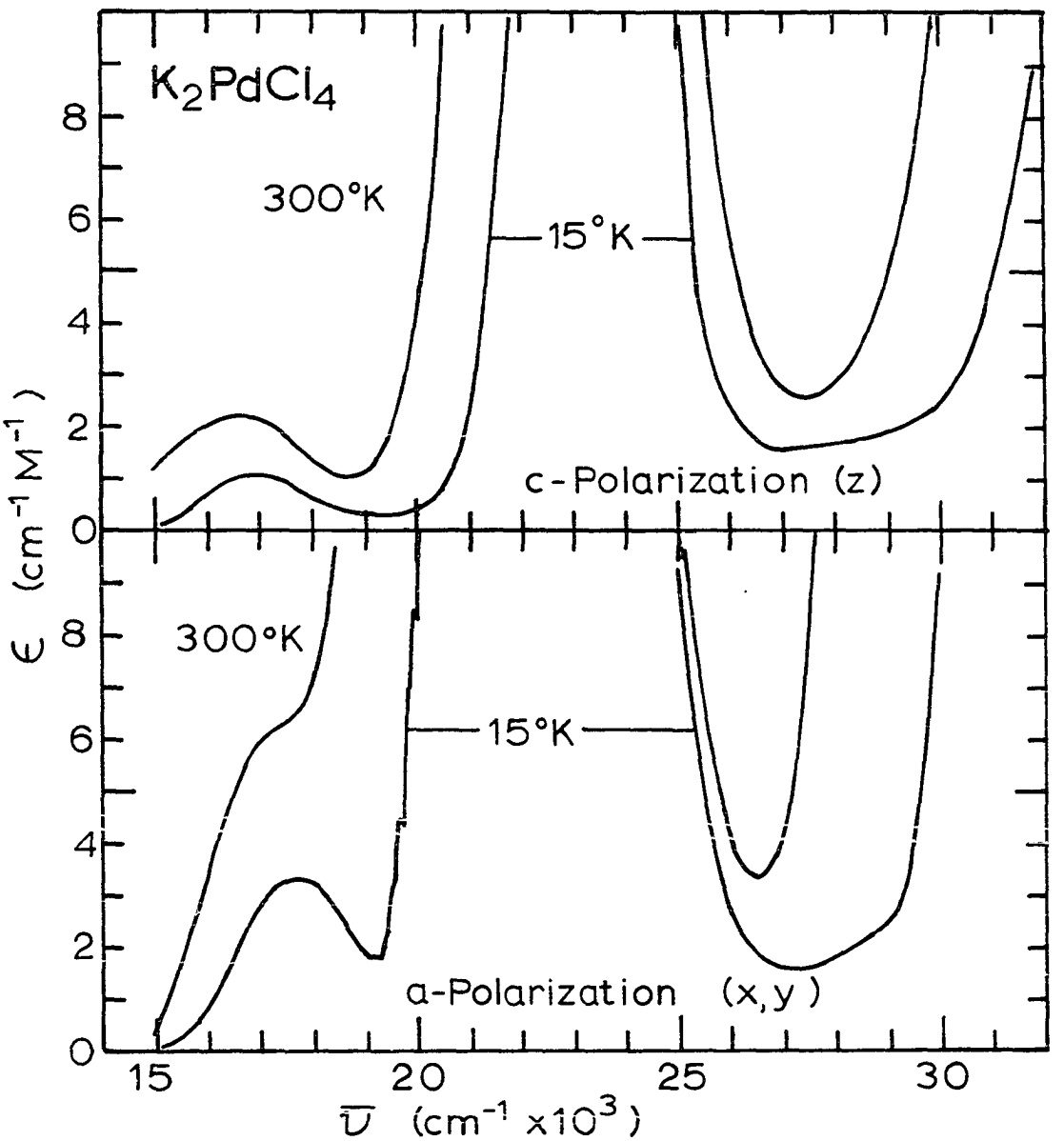

Figure 14. Spectra for a crystal of K_2PdCl_4 which was 155 μ thick.

(54). Day and coworkers (15) also reported a shoulder in the upper limit of their experimentally accessible region. When the spectrum of a thick crystal was traced, a shoulder was observed in the a-polarization; and in particular, the shoulder was observed when the slit width was greater than 1.0. The shoulder was observed at the high absorption limit of our spectral scans. However, when thinner crystals were employed, it was possible to scan through to an absorptivity greater than 440 $cm^{-1}M^{-1}$ which was nearly twice the height of the band at 21,200 cm^{-1} as can be seen in Figure 13. With high absorption in one polarization there can be depolarization of the transmitted light beam. This depolarization is believed to result from scattering by surface imperfections of the crystal. Hence, a small portion of the transmitted light may be of the other polarization. As a consequence, a false shoulder occurs in scans where the absorption in the other polarization turns upward (54). Probably this was the case for the x,y-polarized shoulder at 33,000 cm^{-1} reported by Francke and Moncuit (54) which occurred at a high absorption. The present results indicated that the shoulders reported by the earlier workers at 33,000 cm^{-1} were artificial since it was not observed in the thin crystals.

In Figure 13 a band at 37,000 cm^{-1} was observed in the z-polarization. In the 15°K scan the molar absorptivity decreased from 418 to 388 $cm^{-1}M^{-1}$; however, this decrease was not as pronounced as in the vibronicly excited d↔d transitions.

This band was assigned primarily to the $^1A_{2u} \leftarrow {}^1A_{1g}(b_{1g}-\sigma^*\leftarrow b_{2u}-L\pi)$ transition. The intensity seemed quite low for a fully allowed z-polarized transition. However, Jorgensen (60) has noted that intensities for $\sigma^*\leftarrow\pi$ transitions were low for several transition metal complexes. This appears to be the case for K_2PdCl_4. The small decrease in peak height at lower temperatures can be explained by the presence of other vibronicly allowed transitions near the $^1A_{2u}\leftarrow{}^1A_{1g}$ transition energy.

The solution spectrum at high energies for $PdCl_4^{2-}$ was dominated by two intense bands at 35,700 cm^{-1} (ε = 9,330 $cm^{-1}M^{-1}$) and at 45,000 cm^{-1} (ε = 25,800 $cm^{-1}M^{-1}$). McCaffery and coworkers (18) reported an MCD-A term for the 44,900 cm^{-1} band. Anex and Takeudhi (22) reported the polarized reflectance spectrum for K_2PdCl_4 crystals. They determined that these bands were in-plane or a-polarized. In contrast, the 46,300 cm^{-1} band in K_2PtCl_4 was out-of-plane or c-polarized (22). It can be seen in Figure 13 that the c-polarization was scanned to nearly 44,000 cm^{-1} without a molar absorptivity greater than 450 $cm^{-1}M^{-1}$. The single crystal absorption results imply that these high intensity components in the solution spectrum must be x,y-polarized. Therefore, these dipole allowed bands are assigned to the $^1E_u\leftarrow{}^1A_{1g}(b_{1g}-\sigma^*\leftarrow e_u-L\pi)$ and the $^1E_u\leftarrow{}^1A_{1g}(b_{1g}\leftarrow\sigma^*\leftarrow e_u-L\sigma)$ transitions, respectively.

The ^1E_u assignments were in agreement with those made by Jorgensen (60) and McCaffery et al. (18), but not with that made by Katô (27). Jorgensen suggested that there was a mixing of the two ^1E_u states since they have the same symmetry. The mixing of some sigma character into the state at 35,700 cm^{-1} provided the high intensity for this $\sigma^* \leftarrow L\pi$ transition.

Katô assigned the band at 44,900 cm^{-1} on the basis of the signs of the terms in the MCD spectrum. The wave functions, required for these computations, were based on Slater-type atomic orbitals. Based on a semi-empirical SCF MO calculation, Katô (27) reported the order of transitions in increasing energy as follows:

$$^1E_u \leftarrow {}^1A_{1g}(b_{1g}-\sigma^* \leftarrow e_u-L\pi)$$

$$^1A_{2u} \leftarrow {}^1A_{1g}(b_{1g}-\sigma^* \leftarrow b_{2u}-L\pi)$$

$$^1E_u \leftarrow {}^1A_{1g}(b_{1g}-\sigma^* \leftarrow e_u-L\sigma)$$

$$^1A_{2u} \leftarrow {}^1A_{1g}(a_{2u}-p_z \leftarrow a_{1g}-d_{z^2})$$

$$^1E_u \leftarrow {}^1A_{1g}(a_{2u}-p_z \leftarrow e_g-d_{xz,yz}).$$

His calculations indicated that the sign of the MCD-A term for the $^1E_u \leftarrow {}^1A_{1g}(b_{1g}-\sigma^* \leftarrow e_u-L\pi)$ transition was opposite to the sign for the $^1E_u \leftarrow {}^1A_{1g}(b_{1g}-\sigma^* \leftarrow e_u-L\sigma)$ and the $^1E_u \leftarrow {}^1A_{1g}(a_{2u}-p_z \leftarrow e_g-d_{xz,yz})$ transitions. The sign of the MCD-A term reported (18) for the 44,900 cm^{-1} band agreed with the sign calculated for the $\sigma^* \leftarrow L\pi$ transition (27). Therefore, Katô assigned this

band to the transition state with the lowest calculated energy. Katô's assignment leaves the intense band at 35,700 cm^{-1} without a plausible assignment. Apparently, the MCD-A term for the band at 35,700 cm^{-1} was too small to be measured in the presence of other terms in this vicinity (18).

Messmer, Interrante and Johnson (28) calculated one-electron transition state energies for K_2PdCl_4 by their SCF-Xα-SW method. Relativistic corrections for palladium were not included in this calculation. For K_2PdCl_4 the intermingling of d-like and L-like orbital energy levels was more pronounced than for K_2PtCl_4. It was generally assumed (7,8) that the "d" orbitals were sufficiently well separated in energy from the "ligand" orbitals; however, this may not be the case for the $PdCl_4^{2-}$ ion as the ordering in Figure 11 showed (28).

In Table 5, their calculated (28) transition state energies for $\sigma^* \leftarrow d$ and allowed charge transfer transitions are listed. The experimental assignments from the present work are also listed for immediate comparison. The agreement between the calculated and observed energies for the forbidden $\sigma^* \leftarrow d$ transitions is poor. The values for the charge transfer transitions agreed rather well. Comparison of the SCF-Xα-SW calculations for $PtCl_4^{2-}$ suggests a similar sequence of transitions shifted to lower energy in the case for $PdCl_4^{2-}$. Such a shift is consistent with the smaller ligand field splitting for palladium in comparison to platinum.

Table 5. Comparison of the SCF-Xα-SW calculations and the observed transitions for K_2PdCl_4

Transition	Transition-State Energy		Experiment
	eV	cm^{-1} [a]	cm^{-1}
$^3A_{2g} \leftarrow {}^1A_{1g}(b_{1g}-\sigma^* \leftarrow b_{2g}-d_{xy})$	2.5	20,100	17,000 [b]
$^3E_g \leftarrow {}^1A_{1g}(b_{1g}-\sigma^* \leftarrow e_g-d_{xz,yz})$	2.6	21,000	17,700
$^3B_{1g} \leftarrow {}^1A_{1g}(b_{1g}-\sigma^* \leftarrow a_{1g}-d_{z^2})$	3.2	25,800	
$^1A_{2g} \leftarrow {}^1A_{1g}(b_{1g}-\sigma^* \leftarrow b_{2g}-d_{xy})$	3.5	28,200	21,700
$^1E_g \leftarrow {}^1A_{1g}(b_{1g}-\sigma^* \leftarrow e_g-d_{xz,yz})$	3.5	28,200	23,200
$^1B_{1g} \leftarrow {}^1A_{1g}(b_{1g}-\sigma^* \leftarrow a_{1g}-d_{z^2})$	4.3	34,700	Not observed
$^1E_u \leftarrow {}^1A_{1g}(b_{1g}-\sigma^* \leftarrow e_u-L\pi)$	4.3	34,700	35,720
$^1A_{2u} \leftarrow {}^1A_{1g}(b_{1g}-\sigma^* \leftarrow b_{2u}-L\pi)$	4.6	37,100	37,400
$^1E_u \leftarrow {}^1A_{1g}(a_{1g}-s \leftarrow e_u-L\pi)$	5.4	43,600	
$^1E_u \leftarrow {}^1A_{1g}(b_{1g}-\sigma^* \leftarrow e_u-L\sigma)$	5.5	44,400	44,980
$^1E_u \leftarrow {}^1A_{1g}(a_{2u}-p_z \leftarrow e_g-d_{xz,yz})$	5.7	46,000	

[a] Electron volts were converted to wave numbers and then rounded off to the nearest hundred.

[b] Transitions were not specifically assigned.

The $^3B_{1g}$ and $^1B_{1g}$ states cannot be identified in the single crystal spectra of K_2PdCl_4. From the SCF-Xα-SW calculations (28), the separation between these states was ca. 8,900 cm^{-1} for K_2PdCl_4 and for K_2PtCl_4, it was ca. 6,400 cm^{-1}. Martin and coworkers (17,24) suggested a 12,500 cm^{-1} separation between these states in K_2PtCl_4. The $^3B_{1g}$ state in $PdCl_4^{2-}$ may have been between the $^1A_{2g}$ and ^1E_g states or higher than 28,000 cm^{-1}. Possibly, the $^1B_{1g}$ state was close in energy to the $^1A_{2u}$ state. Any assignments for these states can be only speculative; admittedly, other forbidden transitions may occur in this region.

The similarities between the K_2PdCl_4 and K_2PtCl_4 spectra were striking for the transition to the $^1A_{2g}$ and ^1E_g states. In both compounds well-resolved fine structure was evident on the $^1A_{2g} \leftarrow {}^1A_{1g}$ transition due to the E_u molecular vibrations. The $^1E_g \leftarrow {}^1A_{1g}$ transition was observed in both polarizations with comparable intensity. In K_2PtCl_4 these states were separated by 3,000 cm^{-1} in xy-polarization; whereas, in K_2PdCl_4, they were almost coincident as expected from the MO diagram in Figure 11. In K_2PdCl_4 the d←d in-plane polarized bands were more intense than the out-of-plane bands; the opposite was observed for K_2PtCl_4. The relative increase in intensity was due to the close proximity of the dipole allowed ^1E_u transition at 35,700 cm^{-1} from which the x,y-polarized bands borrowed intensity (1). In contrast to

K_2PtCl_4, no transitions were observed in the single crystal spectra which could be assigned as $^3B_{1g}$, $^1B_{1g} \leftarrow {}^1A_{1g}$. In this work it was not possible to uniquely identify these states but only to suggest that they may be above 28,000 cm^{-1}. In K_2PdCl_4 the high energy transitions were $\sigma^* \leftarrow L$ charge transfer bands. The more intense bands were x,y-polarized; whereas, in K_2PtCl_4 the high energy bands were likely $p \leftarrow d$ transitions with somewhat lower intensities.

C. Potassium Tetrabromopalladate(II)

Spectral studies for potassium tetrabromopalladate(II) were undertaken as a logical extension for the work on K_2PtBr_4 and K_2PdCl_4. The experiments were designed to identify the $d \leftarrow d$ and $d \leftarrow L\pi$ transitions in terms of the selection rules and the vibronic model discussed by Martin (1).

Harris, Livingstone and Reece (57) reported spectrophotometric studies on $PdBr_4^{2-}$ in various non-polar solvents and in nujol mulls. McCaffery et al. (18) reported the MCD spectrum for K_2PdBr_4 in 2M HBr. Earlier experimental work has been extended and the polarized single crystal spectra have been obtained at 300° and 15°K.

In the solution spectrum in Figure 15, a weak component resolved at 16,200 cm^{-1} (ε = 12 $cm^{-1}M^{-1}$) was identified as a spin-forbidden $d \leftarrow d$ transition. The exact assignment of this component was not possible from the solution data alone; however, it was broad, and possibly contained more than one

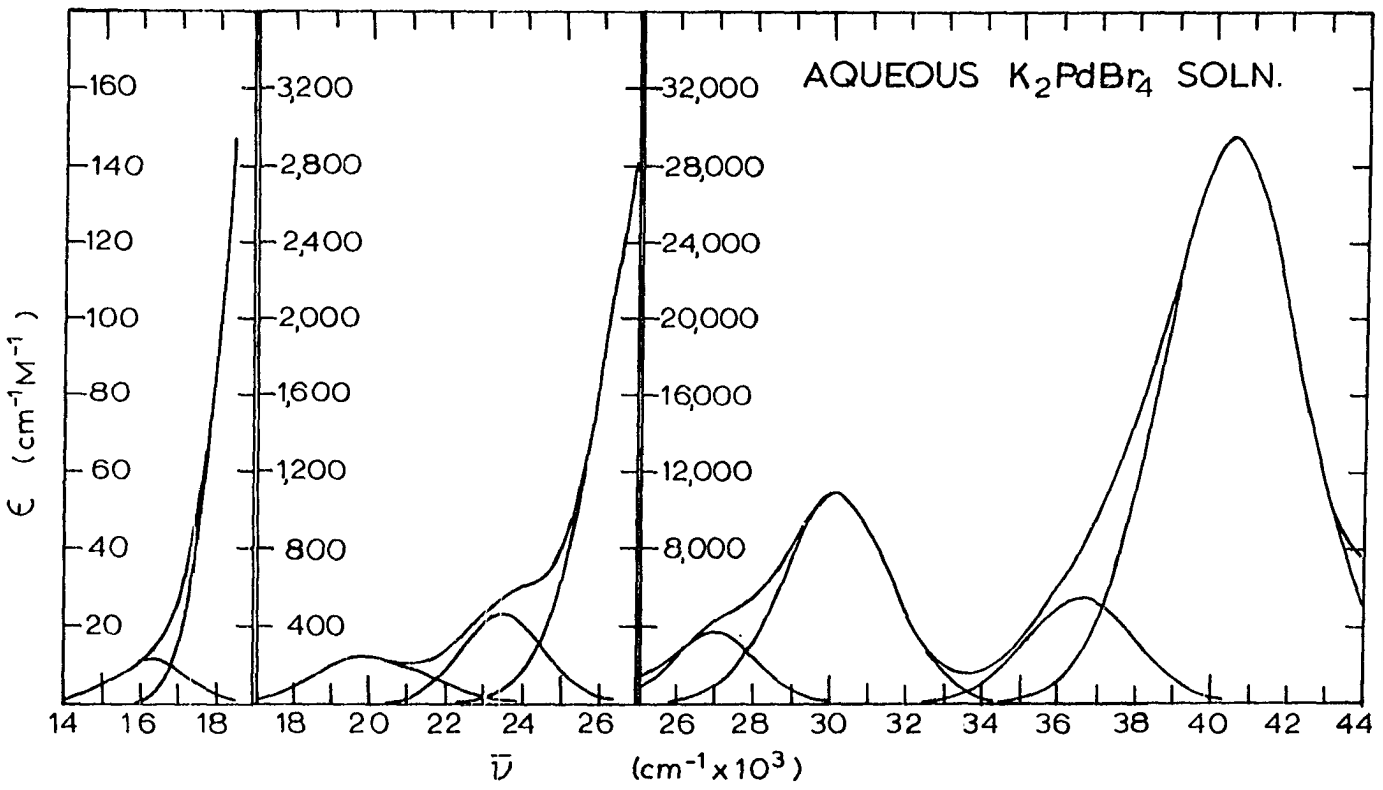

Figure 15. Aqueous spectrum for K_2PdBr_4 in 2M NaBr below 26,000 cm^{-1}. Above 26,000 cm^{-1} the spectrum was obtained in 0.42 M KBr.

transition. Only in very thick crystals were the spin-forbidden transitions observed as shown in Figure 16. In the region below 19,000 cm^{-1}, the absorbance was exceedingly low in the c-polarization. At 15°K two series of vibrational structure were discernible in slow scans and they have been tabulated in Table 6. The first series was centered at 15,700 cm^{-1} and contained seven maxima separated by 162 cm^{-1}. The second series was centered at 17,400 cm^{-1} and the average separation between maxima was 166 cm^{-1}.

The a-polarized spectrum was more intense than the c-polarized. The shoulder seen below 17,000 cm^{-1} at 300°K became a distinct maximum centered at 16,900 cm^{-1} with a molar absorptivity of ca. 5 $cm^{-1}M^{-1}$ at 15°K. In Figure 16, 19 well-resolved vibrational components are observable from 15,400 to 18,380 cm^{-1}. These components are separated by an average of 164 cm^{-1} and have been listed in Table 6. It appeared that a single vibronicly allowed transition was dominant in this region.

In the region below 19,000 cm^{-1}, there were three distinct vibronic transitions. All three had resolvable vibrational structure at 15°K. The structure was representative of the excited state vibrational levels since it was observed in an absorption spectrum. Successive maxima were separated by ca. 164 cm^{-1} which was quite reasonable for the totally symmetric mode, A_{1g}. In the ground state Raman

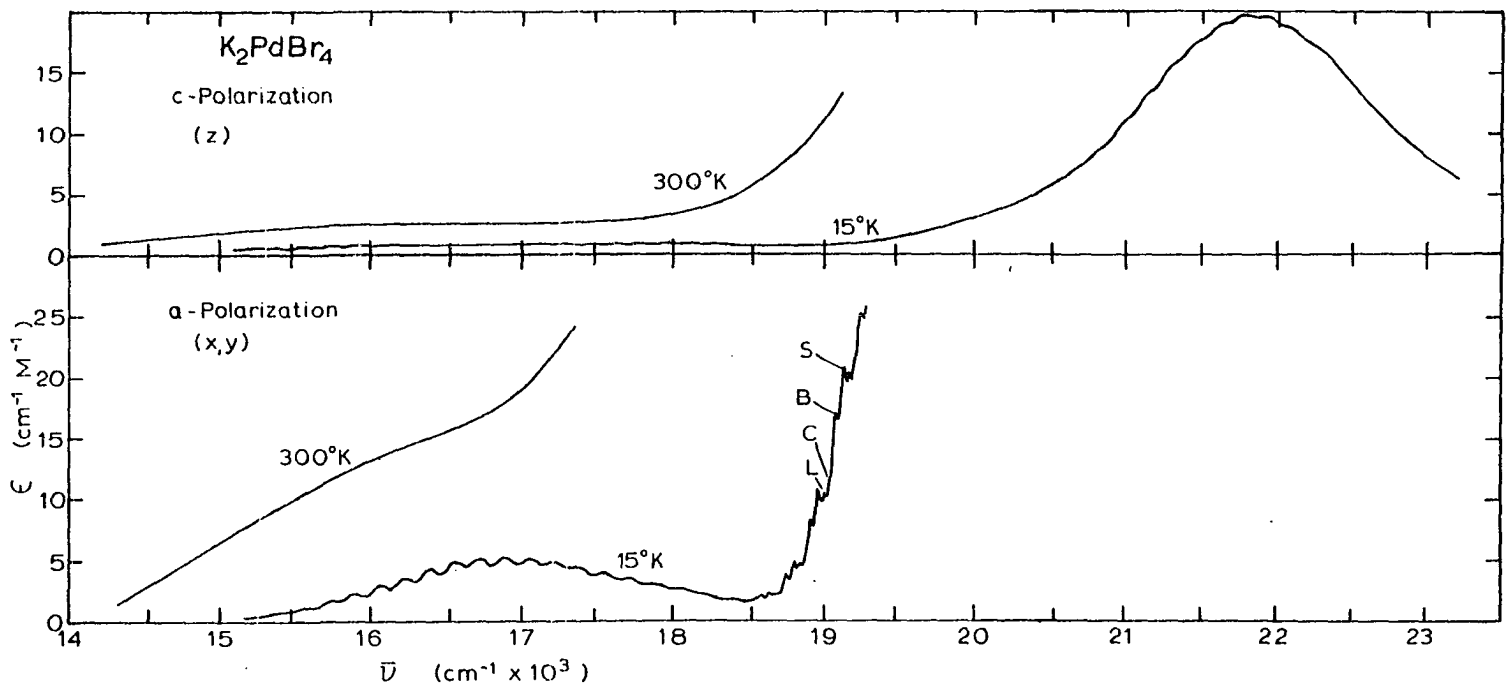

Figure 16. Polarized spectra for K_2PdBr_4. Spectra for z-polarization was for a crystal 205 μ thick. Spectra for x,y-polarization was for a crystal 119 μ thick.

Table 6. Vibrational structure observed at 15°K

Spin-forbidden Transitions		$^1E_g \leftarrow {}^1A_{1g}$ Transition
z-Polarization	x,y-Polarization	z-Polarization
15,240 cm^{-1}	15,400 cm^{-1}	20,340 cm^{-1}
15,410	15,570	20,520
15,580	15,740	20,690
15,730	15,900	20,810
15,910	16,070	20,980
16,060	16,230	21,110
16,220	16,400	21,300
	16,560	21,470
	16,730	21,640
	16,900	21.800
	17,060	21,960
	17,230	22,120
16,770 cm^{-1}	17,390	22,310
16,930	17,550	
17,110	17,720	
17,270	17,890	
17,430	18,050	
17,610	18,200	
17,780	18,380	
17,940		
18,100		

spectrum (61), the A_{1g} frequency was observed at 192 cm^{-1}. The decrease in the A_{1g} frequency was paralleled by similar decreases for K_2PdCl_4 and K_2PtBr_4. The d←d bands observed below 19,000 cm^{-1} were assigned as components of $^3A_{2g} \leftarrow {}^1A_{1g}$ $(b_{1g}-\sigma^* \leftarrow b_{2g}-d_{xy})$ and the $^3E_g \leftarrow {}^1A_{1g}(b_{1g}-\sigma^* \leftarrow e_g-d_{xz,yz})$ transitions. Only three of the seven possible transitions to the $^3A_{2g}$ and ^3E_g states were sufficiently intense to be discerned.

The aqueous spectrum of K_2PdBr_4 was resolved into components by LOGFIT as listed in Table 7. The molar absorptivity for the maximum at 19,800 cm^{-1} was in good agreement with the tabulations of Jorgensen (11) and McCaffery *et al.* (18), but not with those of Harris *et al.* (57). Harris, *et al.*, reported spectra for $(N(C_2H_5)_4)_2PdBr_4$ in acetone, acetonitrile, methanol and nitromethane with extinction coefficients ranging from 400 to 520 $cm^{-1}M^{-1}$ for a maximum at *ca.* 19,300 cm^{-1}. McCaffery *et al.*, observed an MCD-A term at 19,600 cm^{-1} (ε = 316 $cm^{-1}M^{-1}$) and concluded that a transition to a degenerate excited state was included in this band. The $^1E_g \leftarrow {}^1A_{1g}(b_{1g}-\sigma^* \leftarrow e_g-d_{xz,yz})$ transition was suggested.

In the c-polarized spectrum, there was a maximum at 21,300 cm^{-1} with a molar absorptivity of 85 $cm^{-1}M^{-1}$ at 300°K. This was the $^1E_g \leftarrow {}^1A_{1g}$ transition. In the 15°K scan this maximum decreased in intensity to 28 $cm^{-1}M^{-1}$ and shifted

Table 7. Spectral components resolved for K_2PdBr_4

$PdBr_4^{2-}$ Aqueous Spectrum at 300°K			K_2PdBr_4 Crystal Spectra at 15°K						Transition Assignments
			c-z Polarization			a-x,y Polarization			
$\bar{\nu}$, cm^{-1}	ϵ, $cm^{-1}M^{-1}$	Osc.Str.	$\bar{\nu}$, cm^{-1}	ϵ, $cm^{-1}M^{-1}$	Osc.Str.	$\bar{\nu}$, cm^{-1}	ϵ, $cm^{-1}M^{-1}$	Osc.Str.	
			15,700	<1	$\sim 10^{-5}$				
16,210	12	1.3×10^{-4}				16,960	4.8	6.3×10^{-5}	$^3A_{2g} \leftarrow {}^1A_{1g}(b_{1g}-\sigma^* \leftarrow b_{2g}-d_{xy})$
			17,400	<1	$\sim 10^{-5}$				$^3E_g \leftarrow {}^1A_{1g}(b_{1g}-\sigma^* \leftarrow e_g-d_{xz,yz})$
						20,200	177	1.1×10^{-3}	$^1A_{2g} \leftarrow {}^1A_{1g}(b_{1g}-\sigma^* \leftarrow b_{2g}-d_{xy})$
20,050	250	4.1×10^{-3}							
			21,730	33	4.1×10^{-4}				$^1E_g \leftarrow {}^1A_{1g}(b_{1g}-\sigma^* \leftarrow e_g-d_{xz,yz})$
23,450	462	5.3×10^{-3}	Not Present			Not Present			Not $PdBr_4^{2-}$
26,990	3,700	4.1×10^{-2}	26,990	25	2.5×10^{-4}				$\sigma^* \leftarrow L$
30,200	10,600	0.16							$^1E_u \leftarrow {}^1A_{1g}(b_{1g}-\sigma^* \leftarrow e_u-L\pi)$
			30,900	550	6.0×10^{-3}				$^1A_{2u} \leftarrow {}^1A_{1g}(b_{1g}-\sigma^* \leftarrow b_{2u}-L\pi)$
36,500	5,400	8.4×10^{-2}				Intense Absorption			$^3E_u \leftarrow {}^1A_{1g}(b_{1g}-\sigma^* \leftarrow e_u-L\sigma)$
			37,000			Intense Absorption			$\sigma^* \leftarrow L$
40,400	28,900	0.56				Intense Absorption			$^1E_u \leftarrow {}^1A_{1g}(b_{1g}-\sigma^* \leftarrow e_u-L\sigma)$
			43,200			Intense Absorption			$\sigma^* \leftarrow L$

slightly to 21,900 cm^{-1}. The observed intensity reduction was characteristic of vibronicly excited d←d transitions. Because of the vibronic nature of this band, it was possible to record the peak maximum in thick crystals. A spectrum obtained for a crystal large enough to cover a 1 mm pinhole was reproduced in Figure 16. Due to narrow slit widths, some thirteen components were discernible on the $^1E_g \leftarrow {}^1A_{1g}$ z-polarized transition. The components were separated by 162 cm^{-1} as listed in Table 6. This was the first observation of structure on the $^1E_g \leftarrow {}^1A_{1g}$ transition for the series of K_2PtCl_4, K_2PdCl_4 and K_2PtBr_4. Previously (1) in K_2PtCl_4, the absence of structure was explained by an equilibrium configuration other than D_{4h}. Apparently, this was not the case for K_2PdBr_4.

The single crystal spectra of K_2PdBr_4 was recorded in the x,y-polarization at 300 and 15°K as shown in Figure 17. The second maximum was at 19,800 cm^{-1} with a molar absorptivity of 420 $cm^{-1}M^{-1}$ at 300°K. When a crystal was cooled to 15°K, this maximum decreased in intensity to 175 $cm^{-1}M^{-1}$ and vibrational structure was resolved in the low energy region of this band. This transition was absent in the z-polarization. These observations were consistent with the assignment of the $^1A_{2g} \leftarrow {}^1A_{1g}$ transition at 20,120 cm^{-1}. The smaller band at 22,000 cm^{-1} was the $^1E_g \leftarrow {}^1A_{1g}$ transition. The ^1E_g state was observed in both polarizations with

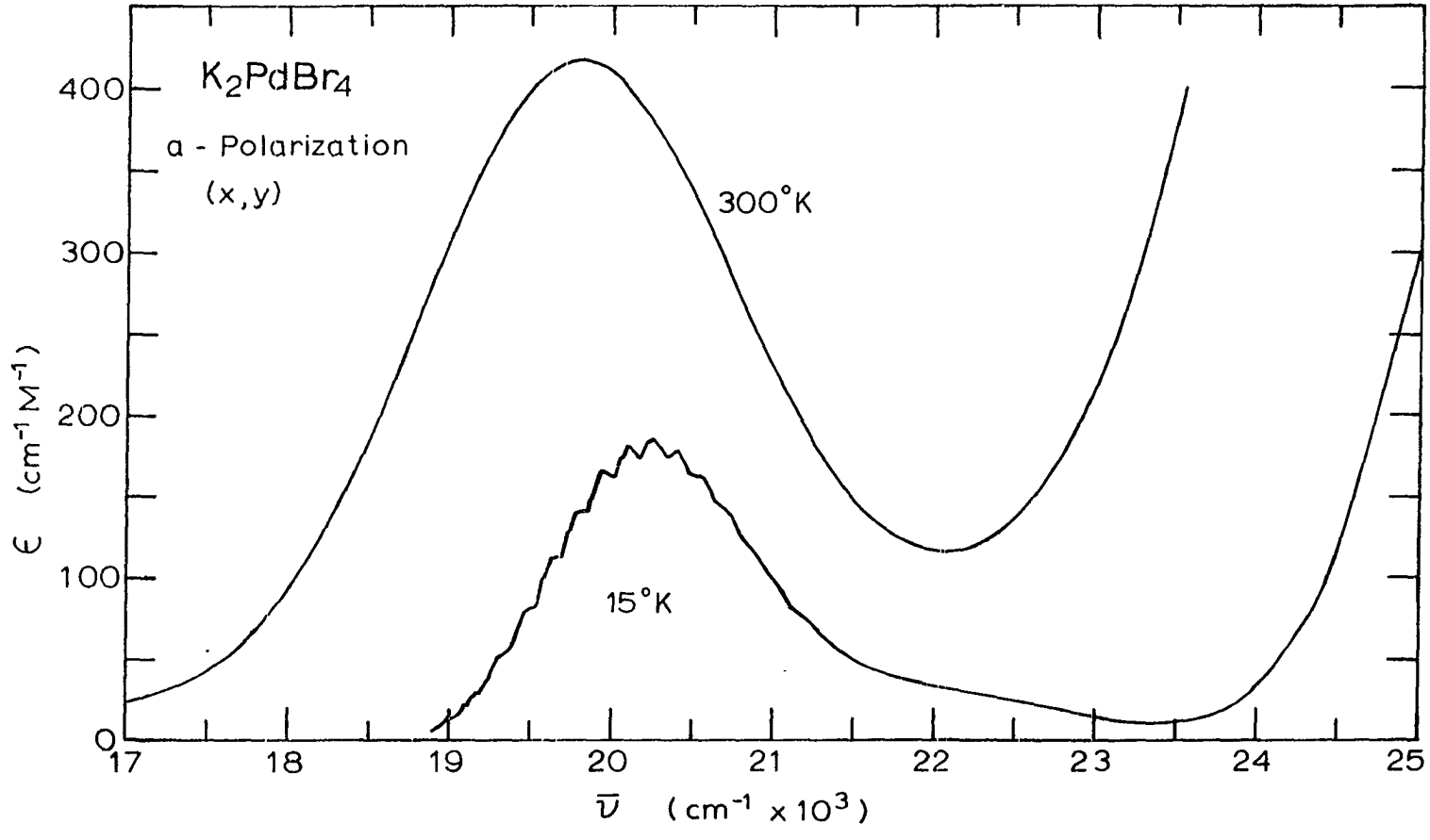

Figure 17. Polarized spectra for K_2PdBr_4. The crystal was 7.7 μ thick.

comparable intensity although it was partially masked by the $^1A_{2g} \leftarrow {}^1A_{1g}$ transition in the x,y-polarization.

The beginning of the $^1A_{2g} \leftarrow {}^1A_{1g}$ transition was observed at 15°K for thick crystals as shown in Figure 16. The absorption was followed to a molar absorptivity of 25 at 19,250 cm^{-1} where the intensity became too great to record. For K_2PdBr_4 the vibrational structure was more detailed than that observed in K_2PtBr_4 (20) or K_2PtCl_4 (17). There were groups of four components which were repeated. In each group there were two intense peaks labeled B and S as shown in Figure 16. A weak shoulder was observed on the lower energy side of B; it was labeled C. A weaker peak was labeled L and was observed at lower energy than C. The C and L components were not observed in the first group as listed in Table 8. The components were periodic; for example, the S peaks were separated on the average by 164 cm^{-1} throughout the resolved structure. In thin crystals the B, S and L peaks were observed from 18,900 to 19,640 cm^{-1} where resolution was lost.

The number of components resolved in the vibrational structure was unique for K_2PdBr_4. For K_2PtBr_4 (20) the $^1A_{2g} \leftarrow {}^1A_{1g}$ structure appeared as a shoulder followed by a peak as was shown in Figure 4. The sharp-line luminescence spectrum observed for Cs_2PtCl_4 in Cs_2ZrCl_6 crystals contained three components which were assigned to the odd vibrations associated

with the $^3B_{1g} \leftarrow {}^1A_{1g}$ transition (21). The $^1A_{2g} \leftarrow {}^1A_{1g}$ transition for Cs_2PtCl_4 was resolved into eleven major peaks and four weak, lattice peaks at 4°K. The $^1A_{2g} \leftarrow {}^1A_{1g}$ transition is excited by E_u vibrations. Hendra (58) reported the infrared spectrum for K_2PdBr_4 with ν_6 = 260 cm^{-1} and ν_7 = 140 cm^{-1} which were stretching and in-plane bending vibrations, respectively. An E_u lattice mode was reported at 85 cm^{-1}. A scheme has been devised to explain the origin of these components observed in K_2PdBr_4.

The basis for this scheme was that the two strong components were due to molecular vibrations. The B peak was assigned to the in-plane bending mode; the S peak was assigned to the in-plane stretch. The B and S components were separated by 55 cm^{-1}; this may be viewed as the difference between ν_6 and ν_7 in the excited state. In the ground state, this difference was 120 cm^{-1}. It seemed reasonable to assume that the stretching mode would decrease in the excited state in view of the decrease for the A_{1g} mode. Possibly, the in-plane bending frequency did not decrease in the excited state. An increase in ν_7 may have been the case since a bending vibration may be restricted by contact with nearest neighbors. The observed 55 cm^{-1} separation is a numerical difference and does not suggest any information about the excited state geometry.

The L component was assigned to the lattice vibration; the first component was observed at 18,520 cm^{-1} as listed in Table 8. There was a question of whether this component was the first L mode or if there was an unobserved L component below 18,430 cm^{-1}. The ground state difference between ν_6 and ν_L was 175 cm^{-1}; and between ν_7 and ν_L, it was 55 cm^{-1}. The separation between S and L was ca. 130 cm^{-1}; and between B and L, it was ca. 70 cm^{-1}. It has been assumed, therefore, that the first observed L component and the second S component had the same excitation of the totally symmetric mode, $\nu_1(A_{1g})$. So the progressions appear to be ordered as listed in Table 8.

The weak shoulder labeled C was assigned to a combination mode having E_u symmetry. This assignment was very subjective since combination bands were not observed in the infrared (58, 59). A combination mode, however, may not be too unlikely since weak overtones of A_{1g} were observed in the resonance Raman experiments (61). The separation between S and C was roughly 75 cm^{-1}; the exact location of the C component was uncertain. The B and C separation was roughly 25 cm^{-1}.

The observed separations for the components appeared reasonable if the frequencies for ν_6 and ν_7 were changed differently in the excited state from their values in the ground state. In the devised scheme, it was assumed that the lattice frequency remains almost unchanged. On the basis of

Table 8. Vibrational structure observed at 15°K for the $^1A_{2g} \leftarrow {}^1A_{1g}$ transition of K_2PdBr_4

Resolved Components (cm^{-1})			
L	B	S	C
	18,430	18,480	18,570
18,520	18,590	18,650	18,730
18,680	18,750	18,800	18,890
18,840	18,910	18,960	19,040
19,000	19,080	19,120	19,200
19,160	19,240	19,290	
19,320	19,400	19,460	
19,490	19,550	19,590	
19,640			

Maxima
19,790
19,950
20,100
20,250
20,400
20,560
20,730
20,880
21,040
21,210

the numerical differences for the components, the following excited state frequencies were obtained: ν_L = 85, ν_C = 299, ν_B = 160 and ν_S = 215 cm^{-1}. The value for ν_C was 135 cm^{-1} plus 164 cm^{-1} which gave 299 cm^{-1} for the combination band. The stretching frequency ν_6 decreased in the excited state; the force constant was reduced about as much as the force constant for the totally symmetric stretching vibration. For the in-plane bending vibration, the force constant increased in the excited state.

In the solution spectrum a component was resolved at 23,450 cm^{-1} with a molar absorptivity of 462 $cm^{-1}M^{-1}$. This component appeared as a shoulder and was more intense than the maximum at 19,800 cm^{-1} as shown in Figure 15. This component could be seen in the spectrum reported by McCaffery *et al.* (18); however, the MCD tracing did not include this region and no mention of this shoulder was made. In the spectra reported by Harris *et al.* (57), there was absorption in this region, too. The a-polarized spectrum was recorded to 25,000 cm^{-1} where it increased steeply without any indication of a shoulder. At 15°K absorbance minima were recorded at 23,600 cm^{-1} in both polarizations. The component resolved at 23,450 cm^{-1} in the solution cannot, therefore, be assigned to the $PdBr_4^{-2}$ species since it does not appear in the crystal spectra with any appreciable intensity.

A similar situation was reported for $PtBr_4^{2-}$ in that the component at 31,500 cm^{-1} could not be assigned (20). In that case, the assignment to a minor solution species - $Pt_2Br_6^{2-}$, was suggested because it had a strong band at that energy. Likewise, in the palladium case, Mason and Gray (62) reported an intense band for $(N(C_2H_5)_4)_2Pd_2Br_6$ at 24,270 cm^{-1} (ε = 3,470 $cm^{-1}M^{-1}$) in acetonitrile solution. In nitromethane, this band was reported (57) at 23,870 cm^{-1} (ε = 5,300 $cm^{-1}M^{-1}$). The reflectance spectrum for $(N(C_2H_5)_4)_2Pd_2Br_6$ was reported by Day, Smith and Williams (63); an intense band was observed at 24,000 cm^{-1}. These data and the possibility of dimer formation in aqueous solution suggested that the 23,450 cm^{-1} component could possibly be due to a small amount of $Pd_2Br_6^{2-}$ present in the solution.

The high energy solution spectrum was dominated by four intense bands at 26,990, 30,200, 36,540 and 40,450 cm^{-1}. The bands at 30,200 and 40,450 cm^{-1} were assigned to the $^1E_u \leftarrow {}^1A_{1g}(b_{1g}-\sigma^* \leftarrow e_u-L\pi)$ and the $^1E_u \leftarrow {}^1A_{1g}(b_{1g}-\sigma^* \leftarrow e_u-L\sigma)$ transitions, respectively. These assignments concur with the MCD spectrum (18). The component at 26,990 cm^{-1} was assigned to the $^3E_u \leftarrow {}^1A_{1g}(b_{1g}-\sigma^* \leftarrow e_u-L\pi)$ transition; this triplet was some 3,200 cm^{-1} lower in energy than the singlet. The band at 36,540 cm^{-1} was assigned to the $^3E_u \leftarrow {}^1A_{1g}(b_{1g}-\sigma^* \leftarrow e_u-L\sigma)$ transition. The intensities of the $^1E_u \leftarrow {}^1A_{1g}$ transitions were greater than those observed for K_2PtBr_4 (20). The

dipole allowed transition intensities were comparable to those observed for K_2PdCl_4.

The intense solution bands must be x,y-polarized since the intensity in the z-polarization was less than 600 $cm^{-1}M^{-1}$ as shown in Figure 18. In the z-polarization at 300°K, a band was observed at 30,700 cm^{-1} with an absorbance of 480 $cm^{-1}M^{-1}$. This transition was dipole allowed since it narrowed and the peak height increased to a molar absorptivity of 550 $cm^{-1}M^{-1}$ at 15°K. This transition was assigned as the $^1A_{2u} \leftarrow {}^1A_{1g}(b_{1g}-\sigma^* \leftarrow b_{2u}-L\pi)$. Since this was a $\sigma^* \leftarrow L\pi$ transition, it was weak compared to other allowed transitions in analogy with the corresponding transition in K_2PdCl_4.

There was a very weak shoulder at 26,990 cm^{-1} in the z-polarization which was resolved at low temperatures. This band was coincident with a strong component resolved from the aqueous spectrum. This band was assigned to a state in the $^3E_u \leftarrow {}^1A_{1g}(b_{1g}-\sigma^* \leftarrow e_u-L\pi)$ transition. This spin-forbidden transition is allowed by virtue of spin-orbit coupling of the bromide ligands. This coupling results in 6 states which transform according to the irreducible representations in D_4'. The $A_{2u}'(\Gamma_2)$ state will mix with the $^1A_{2u}$ state to obtain a nonzero dipole in the z-polarization. This transition was not observed at 300°K due to the close proximity of the $^1A_{2u} \leftarrow {}^1A_{1g}$ transition. Admittedly, this band may contain the $^1B_{1g} \leftarrow {}^1A_{1g}$ transition as well.

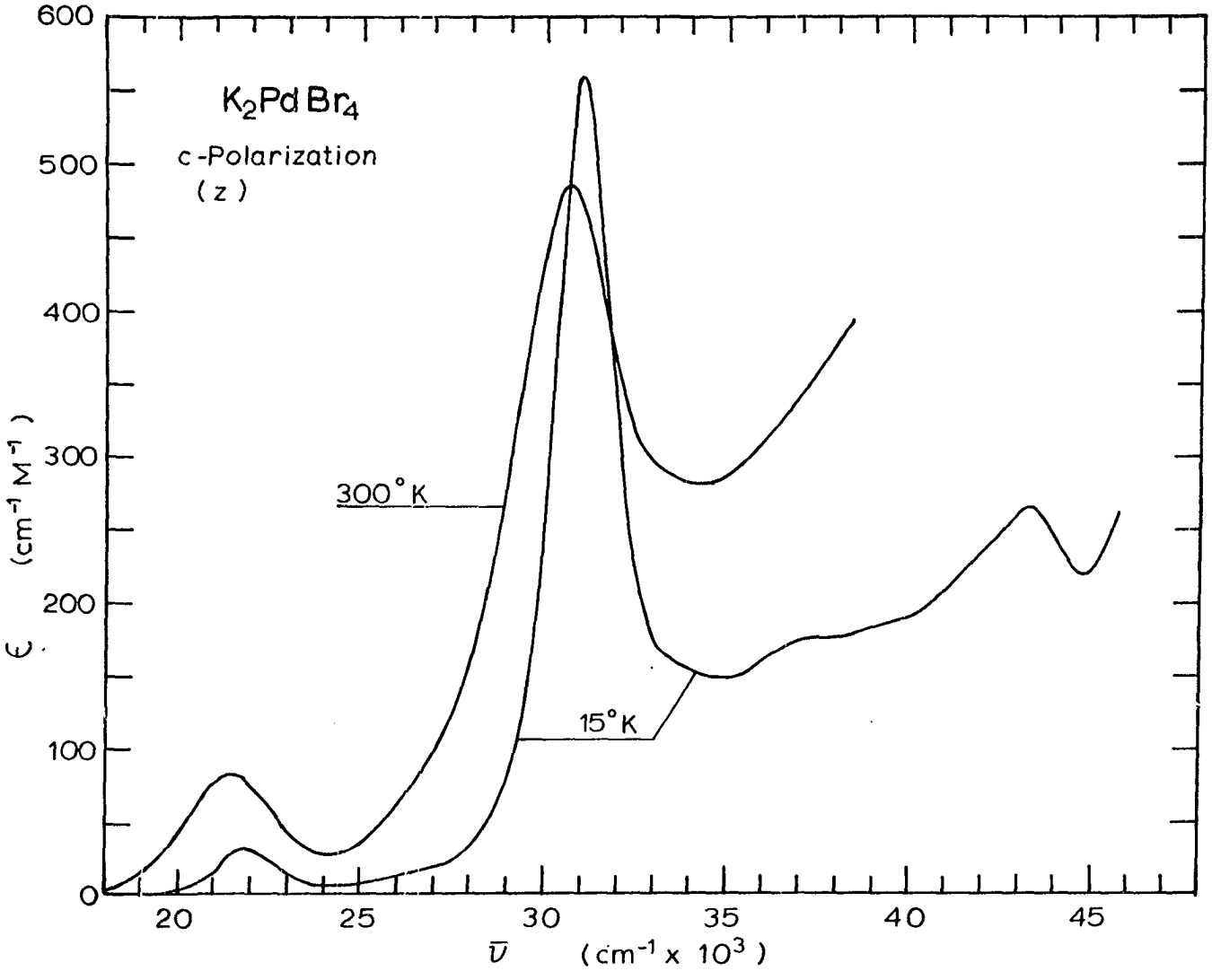

Figure 18. Polarized spectra for K_2PdBr_4. The crystal was 7.7 μ thick.

Beyond 32,000 cm^{-1} in the z-polarization, two distinct bands were observed at 15°K. The bands at 37,000 and 43,200 cm^{-1} were estimated to have a molar absorptivity less than 100 $cm^{-1}M^{-1}$. Care must be taken when characterizing these bands since they were observed near the extreme limits of the experimentally accessible wave lengths. Possibly these were the $^1B_{2u} \leftarrow {}^1A_{1g}(b_{1g}-\sigma^* \leftarrow a_{2u}-L\pi)$ or the $^3E_u \leftarrow {}^1A_{1g}(b_{1g}-\sigma^* \leftarrow e_u-L\sigma)$ or the $^1E_g \leftarrow {}^1A_{1g}(b_{1g}-\sigma^* \leftarrow e_u-L\pi)$ transitions or other forbidden transitions. These transitions do not appear intense enough to be p←d transitions as was the case for K_2PtCl_4. Perhaps, the $^1B_{1g}$ state may lie in this region.

There has not been unanimity in the assignments for square-planar palladium complexes. Katô (27) had assigned the high energy spectrum on the basis of the signs of the MCD curves. Katô assigned the band at 30,100 cm^{-1} to the $^1A_{2u} \leftarrow {}^1A_{1g}(b_{1g}-\sigma^* \leftarrow b_{2u}-L\pi)$ and to the $^1E_u \leftarrow {}^1A_{1g}(a_{2u}-p_z \leftarrow e_g-d_{xz,yz})$ transitions; and the band at 40,500 cm^{-1} was assigned to the $^1E_u \leftarrow {}^1A_{1g}(b_{1g}-\sigma^* \leftarrow e_u-L\pi)$ transition (27). The possibility of a p←d transition as low as 30,100 cm^{-1} seems unlikely since there should then be an intense band in a-polarization at moderate energy. The transitions in K_2PdBr_4 appear to be either σ*←d or σ*←L and not p←d or p←L in origin. The relatively low intensities of a number of the bands observed support this assignment.

The $\sigma^* \leftarrow d$ transitions in K_2PdBr_4 were more intense in the x,y-polarization. The $^1A_{2g}$ and ^1E_g bands were not as well resolved as was the case for K_2PtBr_4. In K_2PdBr_4 these states were separated by 1,700 cm^{-1} compared to 2,400 cm^{-1} in K_2PtBr_4. The vibrational structure observed on the $^1A_{2g} \leftarrow {}^1A_{1g}$ transition was explained. The $^1A_{2g} \leftarrow {}^1A_{1g}$ transition was more intense than the $^1E_g \leftarrow {}^1A_{1g}$ transition; the opposite was true for K_2PtBr_4. In both salts the $^3E_u \leftarrow {}^1A_{1g}$ and $^1E_u \leftarrow {}^1A_{1g}$ (b_{1g}-$\sigma^* \leftarrow e_u$-Lπ) transitions were separated by 3,000 to 4,000 cm^{-1}. As in K_2PtBr_4 and K_2PdCl_4, the high energy bands appeared to be charge transfer transitions.

IV. CRYSTAL STRUCTURE OF POTASSIUM TETRABROMOPLATINATE(II)

A dark red tabular crystal of K_2PtBr_4 was mounted on a glass fiber for X-ray diffraction studies. Precession photographs indicated a primitive tetragonal cell without systematic absences. Long exposures for the zero-layer photographs showed no evidence for a superlattice. These facts suggested that K_2PtBr_4 crystallized in the P 4/m mm space group (D_{4h}^1, No. 123).

The data for K_2PtBr_4 indicated that $\alpha = \beta = \gamma = 90°$; $a = b = 7.350(1)\text{Å}$, $c = 4.326(1)\text{Å}$ with one molecule per cell. A crystal 0.1 x 0.1 x 0.2 mm was used for data collection. Data were taken at ambient temperature on a four-circle diffractometer interfaced with a PDP-15 computer (64). Molybdenum Kα (0.7107Å) radiation was used with a graphite monochromator and a scintillation counter. Data was collected within a 2θ sphere of 60° over the $hk\ell$ and $\bar{h}k\ell$ octants. Three standard non-coplanar reflections were measured periodically to confirm that no crystal decomposition or movement occurred during data collection.

A total of 727 reflections were measured using the step scan technique (65) to obtain integrated intensities. Data were corrected for absorption because the linear absorption coefficient (66) was 353.28 cm^{-1}. Two different programs, OR ABS (67) and TALABS (68), were used to make the absorption corrections. Each program independently created

a data set which was then treated as a separate structure. Data reduction included corrections for Lorentz-polarization as

$$(LP)^{-1} = \text{Sin } 2\theta[(1 + \text{Cos}^2 2\theta_M)/(\text{Cos}^2 2\theta + \text{Cos}^2 2\theta_M)] \quad (13)$$

where θ_M is the glancing angle of the monochromator, 6.1°. Standard deviations (σ_I) in the intensities were estimated from the total count (TC) and the background count (BC) values by

$$(\sigma_I)^2 = TC + BC + (0.03\ TC)^2 + (0.04\ BG)^2 + (0.05\ I)^2. \quad (14)$$

The last three factors were estimates for the non-statistical errors in TC, BG and I. The estimated standard deviation in the structure factor (σ_F) was found by the finite difference method (69).

The equivalent reflections were averaged, and only those with $F_0 > 3\sigma_F$ were considered to be observed. In the OR ABS data, 236 unique reflections were utilized; the TALABS data had 237 unique reflections. For an hkℓ reflection, the transmission factor (70) was rarely the same for TALABS or OR ABS data. Within the same data set, the F_0 for hkℓ and khℓ were not always within 2% of each other. When the intensity of one member of an equivalent pair was zero, averaging was not done and usually the non-zero member was found to be unobserved.

A three-dimensional Patterson (71) map was generated from the data and from this map the atom positions were determined. In the K_2PtBr_4 structure, there were only three

unique atoms because of the high symmetry in the P 4/m mm space group. The Pt atom was located at the origin, the K atoms were at (1/2, 0, 1/2) and (0, 1/2, 1/2), and the Br atoms were at (±x, ±x, 0). These were all special positions and confirmed that K_2PtBr_4 was isostructural with K_2PtCl_4.

The structure was refined by full-matrix least-squares using a local modification of OR FLS (72). The relativistic Hartree-Fock scattering factors of Doyle and Turner (73) were used as modified for real and imaginary parts of anomalous dispersion (74). Because all the atoms were in special positions, OR FLS was patched to permit equivalent positions to be varied jointly. For example, one bromide position was (x, x, 0). The program OR FLS was patched by the subroutine (72) RESET(XYZ) so that the x parameter was varied and y was set equal to the new value of x at the beginning of the next cycle. When each reflection was processed, this subroutine was called for each atom and symmetry card, i.e., 24 times per reflection. Anisotropic temperature factors were restricted by symmetry conditions (75). For Pt and K in special positions, these factors were restricted to $\beta_{11} = \beta_{22} \neq \beta_{33}$, $\beta_{12} = \beta_{13} = \beta_{23} = 0$. For bromine the restricted factors were: $\beta_{11} = \beta_{22} \neq \beta_{33}$, $\beta_{12} \neq 0$, $\beta_{13} = \beta_{23} = 0$. The temperature factor expression had the general form:

$$\exp - \{h^2\beta_{11}+k^2\beta_{22}+\ell^2\beta_{33}+2hk\beta_{12}+2h\ell\beta_{13}+2k\ell\beta_{23}\}. \qquad (15)$$

These symmetry conditions were implemented through the use of the BETA subroutine (72).

The refinement was on F_o and the function minimized was $\Sigma w(|F_o|-|F_c|)^2$ where w was the weight defined as $1/\sigma_F^2$. Refinement resulted in a conventional discrepancy factor, $R = \Sigma||F_o|-|F_c||/\Sigma|F_o|$, and a weighted discrepancy factor $wR = [\Sigma w(|F_o|-|F_c|)^2/\Sigma w|F_o|^2]^{1/2}$. The OR ABS data refined anisotropically to a residual of 0.061 and a weighted residual of 0.094. The TALABS data refined to an R of 0.069 and a wR of 0.115. The final positional and temperature factors were included in Table 9 along with important interatomic distances. The final calculations of structure factors were tabulated in Tables 10 and 11 for OR ABS and TALABS data. Since parameters were not identical, the two data sets were not expected to give the same residual.

The difficulties encountered in solving structures of heavy atoms in highly symmetric space groups were enormous. The major problem was that the atoms sit in special positions precluding parameter variation. X-ray beam absorption occurred to a great extent and correction was not totally possible. Many reflections were of low intensity; occasionally, a reflection was very intense, i.e., 10,000 counts over background. After absorption corrections were made, weaker hkℓ reflections gained their F_o value from calculated transmission factors (70). The two data sets did

Table 9. Final parameters for K_2PtBr_4

	Positional Parameters			Anisotropic Thermal Parameters ($\times 10^3$)		
	x	y	z	β_{11}	β_{33}	β_{12}
Pt[a]	0	0	0	0.775	2.949	0
K	.5	0	.5	1.490	4.218	0
Br	.2341	.2341	0	0.996	4.943	-.085
Pt[b]	0	0	0	0.647	2.604	0
K	.5	0	.5	1.258	4.005	0
Br	.2345	.2345	0	0.840	4.476	-.072

	a	b
Pt-Br	2.434(3)	2.438(4)
Br-K	3.385(2)	3.385(3)
Br^{i}-Br^{ii}	3.442(5)	3.447(5)
Br^{i}-Br^{iii}	3.908(2)	3.902(2)
Br^{ii}-Br^{iv}	4.236(2)	4.236(2)

[a]OR ABS data.

[b]TALABS data.

Table 10. Observed and calculated structure factors (in electrons) for OR ABS data

L = 0

H	K	FO	FC
0	7	3	2
0	8	58	55
10	2	30	29
10	0	8	8
9	0	41	42
7	7	22	21
6	6	49	49
6	7	34	34
6	8	8	8
5	9	19	19
5	7	10	9
5	8	28	28
5	6	10	9
5	5	33	31
5	3	22	20
5	2	11	11
5	1	37	32
4	1	59	59
4	4	102	104
4	5	59	58
4	6	4	4
4	7	2	3
4	8	43	43
4	9	34	33
3	9	11	9
3	8	16	15
3	7	27	26
3	6	46	45
3	4	25	25
3	3	38	38
3	1	35	34
2	2	169	189
2	3	82	82
2	4	9	-5
2	6	87	88
2	7	55	57
2	8	7	5
2	0	18	-18
1	0	69	87
1	9	19	18
1	10	15	14
1	8	30	26
1	7	22	20
1	6	32	32
1	1	45	40
1	2	55	55
0	3	28	32
0	4	141	149
0	5	73	78

L = 1

H	K	FO	FC
0	4	108	104
0	5	72	73
0	3	31	30
1	1	58	96
1	3	72	74
1	2	51	53
1	5	57	57
1	4	55	55
1	6	28	30
1	7	35	34
1	8	28	26
1	9	28	25
2	0	77	-66
2	8	6	-5
2	9	1	-1
2	7	56	53
2	6	61	65
2	4	34	-35
2	5	11	11
2	2	118	126
2	3	77	76
3	5	39	40
3	4	22	24
3	3	66	69
3	6	39	43
3	7	39	37
3	8	14	14
3	9	16	16
4	9	32	31
4	8	33	32
4	6	10	-11
4	7	4	3
4	5	49	55
4	4	67	75
5	5	40	45
5	6	8	9
5	8	25	26
5	7	18	18
6	8	3	2
6	7	31	32
6	6	34	37
7	7	27	26
10	1	15	14
10	2	23	22
0	8	50	41
0	6	19	-20
0	9	65	60
0	0	195	158
0	1	93	79

L = 2

H	K	FO	FC
0	9	34	34
0	0	166	166
0	7	3	3
0	8	46	46
9	3	9	9
8	5	23	23
7	6	27	28
8	2	7	7
8	3	14	13
7	5	8	8
7	1	17	16
7	2	42	44
6	6	40	40
5	5	27	25
5	6	9	9
4	3	22	21
4	5	45	47
4	6	5	4
4	4	77	81
4	8	34	35
4	7	5	4
3	7	21	22
3	6	36	36
3	5	18	18
3	3	32	32
2	2	129	134
2	3	63	63
2	5	11	11
2	6	68	70
1	0	70	63
1	9	17	15
1	8	25	23
1	6	26	27
1	5	30	27
1	4	51	47
1	3	31	28
1	2	45	43
0	2	7	-7
0	3	26	26
1	1	43	34
0	4	107	112
0	5	64	61
0	6	4	3

L = 3

H	K	FO	FC
0	6	8	-9
0	5	46	46
0	4	63	63
1	1	63	54
0	1	49	46
0	3	21	22
1	2	36	33
1	3	48	45
1	5	39	37
1	7	25	24
1	8	17	19
2	0	28	-26
2	7	35	35
2	8	2	-2
2	5	11	10
2	3	70	47
2	3	47	47
2	2	77	73
3	3	42	44
3	6	29	28
4	4	46	47
4	3	18	18
5	3	29	27
4	1	37	36
4	2	17	-15
5	5	31	30
5	4	36	35
6	6	23	24
6	5	9	9
6	1	21	20
6	4	4	-4
6	2	43	40
7	3	26	26
7	5	13	14
7	4	6	5
8	3	11	11
8	4	21	22
8	8	29	28
0	7	4	4
0	0	81	85

L = 4

H	K	FO	FC
0	0	65	73
7	2	24	25
6	4	7	7
6	1	16	16
5	5	15	15
5	3	12	12
5	4	25	26
4	1	26	25
4	4	42	42
5	2	9	10
4	3	15	14
3	6	21	21
3	7	13	13
3	3	20	18
2	1	26	24
3	2	34	32
2	2	71	63
2	6	37	37
2	4	6	4
1	7	10	11
1	5	16	16
1	3	20	18
0	2	4	4
0	1	30	33
1	1	20	21
0	3	17	17
0	4	55	54
0	5	32	32
0	6	6	6

L = 5

H	K	FO	FC
0	5	21	21
0	4	27	26
1	1	20	24
0	2	5	-4
0	3	11	13
1	2	16	17
2	3	20	21
2	2	28	30
1	0	19	21
3	1	22	21
3	3	23	21
4	3	11	11
5	1	19	18
4	4	22	21
4	1	19	17
5	2	8	8
5	3	16	15
0	0	29	34

L = 6

H	K	FO	FC
0	0	21	25
0	1	11	13
1	1	8	10

Table 11. Observed and calculated structure factors (in electrons) for TALABS data

L = 0

H	K	FO	FC
0	7	3	3
0	8	65	63
10	2	34	35
10	0	9	9
9	0	46	48
7	7	25	25
6	6	56	56
6	7	38	39
6	8	9	9
5	9	22	22
5	7	11	10
5	8	32	32
5	6	11	11
5	5	37	34
5	3	25	21
5	1	40	34
5	2	12	12
4	1	61	61
4	4	113	110
4	5	66	62
4	6	4	5
4	7	3	4
4	8	49	50
4	9	38	39
3	9	12	12
3	8	17	17
3	7	31	29
3	6	51	49
3	4	28	27
3	3	40	39
3	1	35	35
2	2	164	192
2	3	84	83
2	4	9	-5
2	6	94	95
2	7	61	62
2	8	8	6
2	0	17	-18
1	0	68	87
1	9	22	20
1	10	17	18
1	8	33	30
1	7	24	22
1	6	35	34
1	2	51	56
1	1	38	40
0	1	61	87
0	3	30	34
0	4	153	154
0	5	81	81

L = 1

H	K	FO	FC
0	4	120	107
0	5	81	76
0	3	34	31
1	1	106	97
1	2	56	54
1	5	62	60
1	4	60	57
1	3	79	76
1	7	38	38
1	6	31	33
1	9	32	29
1	8	31	29
2	9	2	2
2	0	82	-67
2	8	6	-6
2	6	67	70
2	7	62	58
2	5	12	12
2	4	38	-37
2	2	130	128
2	3	85	78
3	4	25	26
3	3	74	72
3	7	44	42
3	6	43	47
3	5	43	44
3	8	16	17
3	9	19	20
4	8	37	38
4	9	36	37
4	7	5	4
4	6	11	-12
4	5	55	59
4	4	76	80
5	5	45	49
5	7	21	21
5	6	9	11
5	8	29	31
6	8	3	3
6	7	35	38
6	6	37	42
7	7	30	31
7	0	6	4
10	1	17	17
10	2	26	27
0	8	56	47
0	6	21	-21
0	9	51	46
0	0	205	159
0	1	95	79

L = 2

H	K	FO	FC
0	9	38	40
0	0	174	168
0	7	3	4
0	8	50	52
9	3	10	11
8	2	8	8
8	3	16	16
8	5	25	27
7	6	31	33
7	5	10	10
7	2	47	49
7	1	19	18
6	6	46	47
5	5	30	27
5	6	10	11
4	3	25	23
4	4	87	88
4	5	50	51
4	6	6	5
4	7	5	6
4	8	38	41
3	7	24	25
3	5	20	19
3	6	40	40
3	3	36	33
2	2	141	139
2	3	70	65
2	5	13	12
2	6	76	77
1	9	18	18
1	0	75	64
1	8	27	26
1	6	29	29
1	5	33	29
1	3	34	30
1	4	56	49
1	2	48	44
0	2	8	-7
0	3	28	27
1	1	45	34
0	4	119	117
0	5	71	64
0	6	4	3

L = 3

H	K	FO	FC
0	6	9	-10
0	5	52	50
0	4	70	67
0	1	50	48
0	3	23	23
1	2	38	35
1	1	61	56
1	5	42	40
1	3	51	47
1	7	27	27
1	8	19	22
2	0	31	-28
2	7	39	40
2	8	2	-2
2	5	12	12
2	3	78	50
2	3	52	50
2	2	84	77
3	3	47	46
3	6	32	32
4	4	52	51
4	3	20	20
4	2	19	-16
4	1	40	38
5	3	32	30
5	4	40	39
5	5	35	34
6	6	26	29
6	2	48	45
6	4	5	-4
6	5	10	11
6	1	23	23
7	5	15	17
7	4	7	6
7	3	29	30
8	3	13	14
8	4	23	26
0	8	32	33
0	7	5	6
0	0	87	88

L = 4

H	K	FO	FC
8	0	72	78
7	2	27	29
6	1	18	19
6	4	7	7
5	5	17	18
5	3	13	14
5	4	28	29
5	2	10	11
4	1	29	27
4	4	48	47
4	3	17	16
3	6	24	24
3	7	15	16
3	3	22	20
2	2	73	68
3	2	36	35
2	1	26	26
2	6	41	42
2	4	6	4
1	5	18	18
1	7	11	13
1	3	21	19
0	2	5	3
0	1	33	34
1	1	21	22
0	3	20	18
0	4	62	59
0	5	36	35
0	6	7	7

L = 5

H	K	FO	FC
0	5	24	24
0	4	30	30
1	1	22	26
0	2	5	-5
0	3	13	14
1	2	17	19
2	3	22	24
1	0	21	23
3	1	24	24
2	2	30	34
3	3	25	23
4	3	12	13
4	4	24	24
4	1	20	20
5	1	21	21
5	2	9	9
5	3	17	17
0	0	32	32

L = 6

H	K	FO	FC
0	0	24	29
1	1	9	11
0	1	13	15

not refine to the same discrepancy factor; however, either procedure appeared satisfactory. The convergence of the refinement for both data sets supported the selection of the centric P 4/m mm space group for K_2PtBr_4.

The square-planar $PtBr_4^{-2}$ ions were packed in the unit cell as shown in Figure 19. The Br^i-Br^{ii} distance was 3.44Å which was shorter than expected since the ionic radius for bromide ions in ionic lattices is 1.95Å (76). This shortening results from the bonding between the platinum and bromine ligands. For adjacent anions, the Br^i-Br^{iii} distance was 3.90Å as expected for ionic bromides (76). The Br^{ii}-Br^{iv} distance was larger than expected from a hard sphere packing model, possibly because the $PtBr_4^{-2}$ ions were separated by potassium ions. The Pt-Br^i distance was 2.43Å; the K-Br^i distance was 3.38Å which was larger than 3.28Å, the sum of ionic radii. Each potassium was surrounded by a rectangular parallelepiped of bromides.

Crystals of potassium tetrabromoplatinate(II) were shown to be tetragonal and isostructural with K_2PtCl_4, K_2PdCl_4 (53) and K_2PdBr_4 (25). Physical data obtained through X-ray diffraction studies on these four compounds showed that the bromide salts had unit cells 24-30Å^3 larger than the chloride salts. In all compounds the anions were separated by more than 4.1Å in the c direction as indicated in Table 12.

Figure 19. Perspective view of the unit cell for K_2PtBr_4.

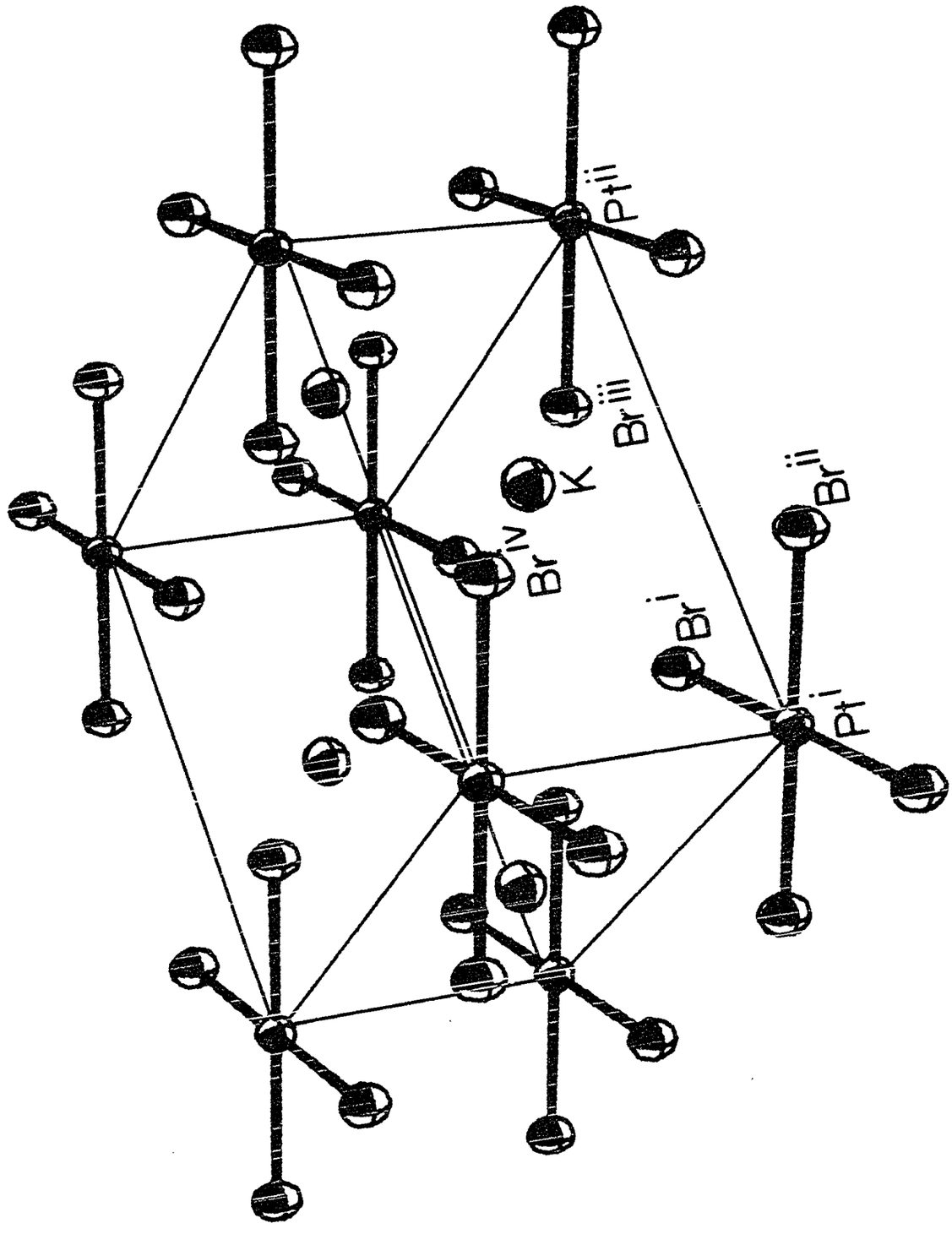
Pt
Br
K
Br
Br
Br
Pt

Table 12. Comparison of data for K_2MX_4 where M is Pt or Pd and X is Cl or Br

	K_2PtCl_4	K_2PdCl_4	K_2PtBr_4[a]	K_2PdBr_4
a(Å)	7.025(3)	7.075(5)	7.350(3)	7.409(12)
c(Å)	4.144(2)	4.112(3)	4.236(2)	4.309(7)
Vol Å^3	204.5	205.8	228.8	236.5
ρ_{calc}(g/cc)	3.35	2.67	4.19	3.54
M-X(Å)	2.316(3)	2.313(3)	2.434(3)	2.444(3)
K-Br	3.239(2)	3.243(2)	3.385(2)	3.396(3)
X^i-X^{ii}	3.266(2)	3.271(2)	3.442(5)	3.456(6)
X^i-X^{iii}	3.757(2)	3.804(2)	3.908(2)	3.953(7)
X^{ii}-X^{iv}	4.144(3)	4.112(2)	4.236(2)	4.309(7)
μ(cm^{-1})	220	40.9	353.3	206.7
R	.015[b]	.041[b]	0.061	.040
Reference	53	53	--	25

[a]OR ABS data.

[b]Extensive data weighting procedures.

V. SUMMARY

The absorption spectra for tetraammineplatinum(II) tetrachloroplatinate(II), potassium tetrachloropalladate(II), and potassium tetrabromopalladate(II) have been recorded at 300° and 15°K for light polarized in the a- and c- directions. Crystals of anhydrous K_2PtBr_4 have the tetragonal K_2PtCl_4 structure with a = 7.350(3)Å and c = 4.236(2)Å. The Pt-Br bond length is 2.434(3)Å.

In Magnus' green salt the bands at 16,000 cm^{-1} in c-polarization and at 25,000 cm^{-1} in a-polarization appear to be vibronicly excited. The $\sigma^* \leftarrow d$ transitions for $Pt(NH_3)_4^{2+}$ and $PtCl_4^{2-}$ have been red shifted by coulombic interactions in the solid state. The 34,500 cm^{-1} band has been assigned to the $^1A_{2u} \leftarrow {}^1A_{1g}(a_{2u}\text{-}p_z \leftarrow a_{1g}\text{-}d_{z^2})$ transition which represents a red shift of 16,000 to 20,000 cm^{-1}. The c-polarized bands in MGS have been red shifted more than the a-polarized bands. For MGS the Pt-Pt separation is 3.24Å and crystal effects provide striking changes in some transition energies. For the square-planar palladium(II) complexes in this thesis, the ions are separated by more than 4.0Å and extended interactions have negligible influence on the electronic transitions.

The energy states for K_2PdCl_4 and K_2PdBr_4 are shown for comparison in Figure 20. For both salts the $^1A_{2g}$ and ^1E_g states are separated by less than 2,000 cm^{-1}. The

Figure 20. Comparison for excited states of K_2PdCl_4 and K_2PdBr_4. The length of the line for each state is proportional to log ε from the crystal spectra at 15°K. The dashed lines are proportional to log ε from the solution spectra.

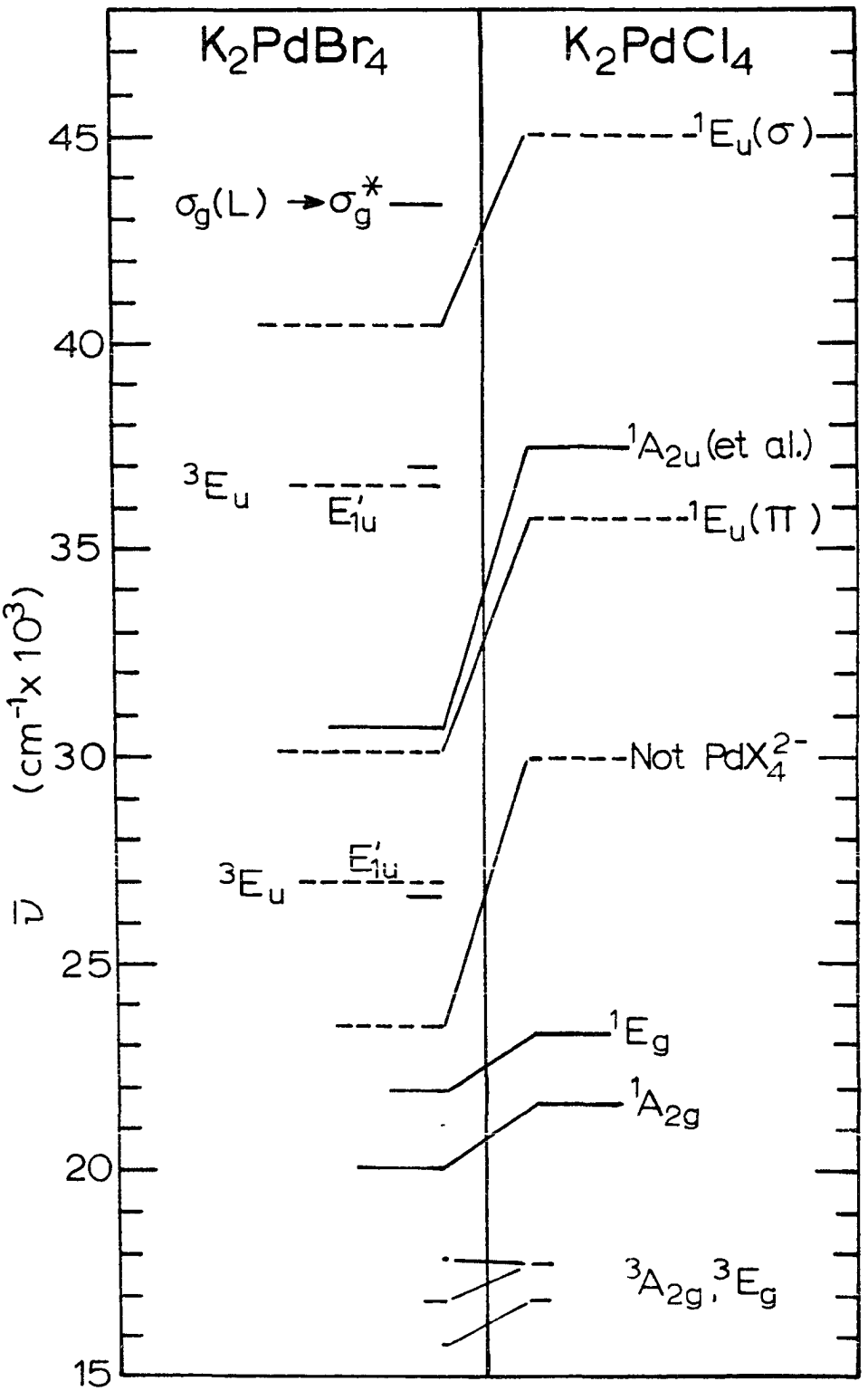
K2PdBr4
K2PdCl4
45
40
35
30
25
20
15
ν̄ (cm-1x 10³)
σg(L) → σg*
3Eu
E'1u
3Eu
E'1u
1Eu(σ)
1A2u(et al.)
1Eu(π)
Not PdX4 2-
1Eg
1A2g
3A2g, 3Eg

corresponding spectral bands are not clearly resolved in x,y-polarization. For K_2PtCl_4 and K_2PtBr_4, these states are separated by ca. 2,500 cm^{-1} and the transitions are clearly resolved in the x,y-polarization. The separation between the states reflects the π-antibonding character of d_{xy} and the $d_{xz,yz}$ orbitals. The separation indicates somewhat less π-character in the palladium salts. These states are ca. 1,200 cm^{-1} lower in energy for K_2PdBr_4 than for K_2PdCl_4. This red shift may be explained by the weaker ligand field for bromide ligands or perhaps less antibonding character in the $d_{x^2-y^2}$ orbital. The $^1B_{1g} \leftarrow {}^1A_{1g}$ transition is not assigned in either of the palladium(II) complexes.

The spin-forbidden σ*←d transitions in K_2PdCl_4 and K_2PdBr_4 were weak compared to these transitions in K_2PtCl_4 and K_2PtBr_4. For the $^3A_{2g}$ and ^3E_g states, none of the components were identified. Vibrational structure was more pronounced for K_2PdBr_4.

For K_2PdBr_4 the $^1A_{2u}$ and ^1E_u states lie about 4,500 to 6,500 cm^{-1} lower in energy than they do for K_2PdCl_4. This is a fairly large red shift, but it is consistent with intraionic σ*←L charge transfer transitions. The $^1A_{2u} \leftarrow {}^1A_{1g}$ transition has low intensity; whereas, the two $^1E_u \leftarrow {}^1A_{1g}$ transitions have relatively high intensities as expected. The ^3E_u states lie some 3,000 to 4,000 cm^{-1} below the ^1E_u states for K_2PdBr_4.

The spectra for K_2PdCl_4 and K_2PdBr_4 indicate that the high energy bands are essentially charge transfer transitions.

For K_2PtBr_4 the transitions are primarily charge transfers and the higher energy bands in solution are of mixed character. For K_2PtCl_4 the spectra is different since the high energy, intense band at 46,300 cm^{-1} is z-polarized (22) and can be assigned to the $^1A_{2u} \leftarrow {}^1A_{1g}(a_{2u}\text{-}p_z \leftarrow a_{1g}\text{-}d_{z^2})$ transition. The low energy $\sigma^* \leftarrow d$ transitions for all four salts appear to be excited by molecular vibrations. The intensities of these forbidden transitions are influenced by the proximity of the dipole allowed transitions.

VI. BIBLIOGRAPHY

1. D. S. Martin, Jr., Inorg. Chim. Acta Rev., 5, 107 (1971).

2. D. S. Martin, Jr., 167th National Meeting of the American Chemical Society, Los Angeles, Calif., April 1974, No. 198 INOR.

3. R. G. Dickinson, J. Amer. Chem. Soc., 44, 2404 (1922).

4. E. Staritzky, Anal. Chem., 28, 915 (1956)

5. J. Chatt, G. O. Gamlen and L. E. Orgel, J. Chem. Soc., 1958, 486.

6. R. F. Fenske, D. S. Martin, Jr., and K. Ruedenberg, Inorg. Chem., 1, 441 (1962).

7. H. B. Gray and C. J. Ballhausen, J. Amer. Chem. Soc., 85, 260 (1963).

8. H. Basch and H. B. Gray, Inorg. Chem., 6, 365 (1967).

9. F. A. Cotton and C. B. Harris, Inorg. Chem., 6, 369 (1967).

10. S. Yamada, J. Amer. Chem. Soc., 73, 1182 (1951).

11. C. K. Jorgensen, Adv. Chem. Physics, 5, 33 (1963).

12. D. S. Martin, Jr., and C. A. Lenhardt, Inorg. Chem., 3, 1368 (1964).

13. O. S. Mortensen, Acta Chem. Scand., 19, 1500 (1965).

14. D. S. Martin, Jr., M. A. Tucker and A. J. Kassman, Inorg. Chem., 4, 1682 (1965).

15. P. Day, A. F. Orchard, A. J. Thompson and R.J.P. Williams, J. Chem. Phys., 42, 1973 (1965).

16. D. S. Martin, Jr., J. G. Foss, M. E. McCarville, M. A. Tucker and A. J. Kassman, Inorg. Chem., 5, 491 (1966).

17. D. S. Martin, Jr., M. A. Tucker and A. J. Kassman, Inorg. Chem., 5, 1298 (1966).

18. A. J. McCaffery, P. N. Schatz and P. N. Stephens, J. Amer. Chem. Soc., 90, 5730 (1968).

19. A.B.P. Lever, "Inorganic Electronic Spectroscopy," Elsevier Publishing Co., New York, N.Y., 1968, p. 124.

20. R. F. Kroening, R. M. Rush, D. S. Martin, Jr., and J. C. Clardy, Inorg. Chem., 13, 1366 (1974).

21. H. H. Patterson, J. J. Godfrey and S. M. Khan, Inorg. Chem., 11, 2872 (1972).

22. B. G. Anex and N. Takeudhi, J. Amer. Chem. Soc., 96, 4411 (1974).

23. D. S. Martin, Jr., L. D. Hunter, R. Kroening and R. F. Coley, J. Amer. Chem. Soc., 93, 5433 (1971).

24. R. F. Kroening, L. D. Hunter, R. M. Rush, J. C. Clardy and D. S. Martin, Jr., J. Phys. Chem., 77, 3077 (1973).

25. D. S. Martin, Jr., J. L. Bonte, R. M. Rush and R. A. Jacobson, submitted for publication in Acta Cryst.

26. R.H.B. Maise, P. G. Owston and A. M. Wood, Acta Cryst., B28, 393 (1972).

27. H. Katô, Bull. Chem. Soc. Japan, 45, 1281 (1972).

28. R. P. Messmer, L. V. Interrante and K. H. Johnson, J. Amer. Chem. Soc., 96, 3847 (1974).

29. H. L. Grube, "Handbook of Preparative Inorganic Chemistry," Vol. 2, George Brauer, Ed., Academic Press, New York, N.Y., 1965, pp 1580-1584.

30. G. B. Kauffman and J. H. Tsai, "Inorganic Synthesis," Vol. VIII, H. F. Holtzclaw, Jr., Ed., McGraw-Hill Book Co., New York, N.Y., 1966, p 235.

31. L. F. Grantham, T. S. Ellerman and D. S. Martin, Jr., J. Amer. Chem. Soc., 77, 2965 (1955).

32. L. D. Hunter, "Polarized absorption electronic spectra for single crystals of dichloro(ethylenediamine)-platinum(II)," Unpublished Ph.D. Thesis, Library, Iowa State University of Science and Technology, Ames, Iowa, 1971, p 82.

33. R. F. Kroening, "Polarized crystal absorption spectra for dibromo(ethylenediamine)platinum(II)," Unpublished M.S. Thesis, Library, Iowa State University of Science and Technology, Ames, Iowa, 1973, p 34.

34. E. E. Wahlstrom, "Optical Crystallography," John Wiley and Sons, Inc., New York, N.Y., 1969, pp 102-109.

35. M. Born and E. Wolf, "Principles of Optics," 2nd ed., Pergamon Press, Oxford, England, 1964, p 324f.

36. E. G. Cox, F. W. Pinkard, W. Wardlaw and G. H. Preston, J. Chem. Soc., 2527 (1932).

37. L. I. Elding, Inorg. Chim. Acta, 4, 647 (1972).

38. D. B. Siano and D. E. Metzler, J. Chem. Phys., 51, 1856 (1969).

39. G. Magnus, Annalen der. Physik., 14, 239 (1928).

40. J. R. Miller, J. Chem. Soc., 713 (1965).

41. J. Atoji, J. W. Richardson and R. E. Rundle, J. Amer. Chem. Soc., 79, 3017 (1957).

42. B. G. Anex, M. E. Ross and M. W. Hedgecock, J. Chem. Phys., 46, 1090 (1967).

43. P. Day, A. F. Orchard, A. J. Thompson and R.J.P. Williams, J. Chem. Phys., 43, 3763 (1965).

44. L. V. Interrante and F. P. Bundy, Inorg. Chem., 10, 1169 (1971).

45. J. C. Zahner and H. G. Drickamer, J. Chem. Phys., 33 1625 (1960).

46. R. P. Messmer and L. V. Interrante, Inorg. Chem., 10, 1174 (1971).

47. H. Isci and W. R. Mason, Inorg. Nucl. Chem. Letters, 8, 885 (1972).

48. J. R. Miller, J. Chem. Soc., 4452 (1961).

49. R. A. Jacobson and J. E. Benson, Iowa State University, Ames, Iowa, private communication, 1970.

50. J.L.H. Batiste, "Charge transfer spectra of square-planar d^8 transition metal complexes," Unpublished Ph.D. Thesis, Library, University of Windsor, Windsor, Ontario, Canada, 1970.

51. D. S. Martin, Jr., R. M. Rush, R. F. Kroening and P. F. Fanwick, Inorg. Chem., 12, 301 (1973).

52. A. Gutbier and A. Krell, Chem. Ber., 38, 2385 (1905).

53. R.H.B. Maise, P. G. Owston and A. M. Wood, Acta Cryst, B28, 393 (1972).

54. E. Francke and C. Moncuit, C. R. Acad. Sci., Ser. B, 271, 741 (1970).

55. E. Tondello, L. DiSipio, G. DeMichelis and L. Oleari, Inorg. Chim. Acta, 5, 305 (1971).

56. K. H. Johnson, Advan. Quantum Chem., 7, 143 (1973).

57. C. M. Harris, S. E. Livingstone and I. H. Reece, J. Chem. Soc., 1505 (1959).

58. P. Hendra, J. Chem. Soc. A., 1298 (1967).

59. C. H. Perry, D. P. Athans, E. F. Young, J. R. Durig and B. R. Mitchell, Spectrochima. Acta, 23A, 1137 (1967).

60. C. K. Jorgensen, Prog. Inorg. Chem., 12, 130 (1970).

61. H. Hamaguchi, I. Haroda and T. Shimanouchi, Chem. Letters, 1, 1049 (1973).

62. W. R. Mason and H. B. Gray, J. Amer. Chem. Soc., 90, 5722 (1968).

63. P. Day, M. J. Smith and R.J.P. Williams, J. Chem. Soc. A, 668, (1968).

64. D. R. Schroeder and R. A. Jacobson, Inorg. Chem., 12, 210 (1973).

65. L. E. Alexander and G. S. Smith, Acta Cryst., 15, 983 (1962).

66. "International Tables of X-Ray Crystallography," Vol. III, 2nd ed., Kynoch Press, Birmingham, England, 1968, p 157.

67. D. J. Wehe, W. R. Busing and H. A. Levy, "OR ABS, A Fortran Program for Calculating Single Crystal Absorption Corrections," USAEC Report ORNL-TM-229, Oak Ridge National Laboratory, Oak Ridge, Tennessee, 1962.

68. J. D. Scott, Queen's University, Kingston, Ontario, Canada, private communication, 1971.

69. S. L. Lawton and R. A. Jacobson, Inorg. Chem., 7, 2124 (1968).

70. J. DeMeulenair and H. Tompa, Acta Cryst., 19, 1014 (1965).

71. C. R. Hubbard, C. O. Quicksall and R. A. Jacobson, "The Fast Fourier Algorithm and the Programs ALFF, ALFFDP, ALFFPROJ, ALFFT and FRIEDEL," USAEC Report IS-2625, Ames Laboratory, Iowa State University, Ames, Iowa, 1971.

72. W. R. Busing, K. O. Martin and H. A. Levy, "OR FLS, A Fortran Crystallographic Least-Squares Program," USAEC Report ORNL-TM-305, Oak Ridge National Laboratory, Oak Ridge, Tennessee, 1962.

73. P. A. Doyle and P. S. Turner, Acta Cryst., A24, 390 (1968).

74. H. P. Hansen, F. Herman, J. D. Lea and S. Skillman, Acta Cryst., 17, 1040 (1964).

75. H. A. Levy, Acta Cryst., 9, 679 (1956).

76. B. E. Douglas and D. H. McDaniel, "Concepts and Models of Inorganic Chemistry," Blaisdell Publishing Co., Waltham, Mass., 1965, p 109.

VII. ACKNOWLEDGMENTS

The author wishes to express her gratitude to Dr. Don S. Martin, Jr. for his guidance, interest and encouragement during this work; to the members of Radiochemistry Group II for their assistance (and moral support) during the tenure of this research.